Tiago Neves Lopes

Fotomultiplicador gasoso sensível ao UVV com resolução em posição

VUV single photon Gas Photomultiplier with position capability

Tiago
Neves Lopes

Fotomultiplicador gasoso sensível ao UVV com resolução em posição

VUV single photon Gas Photomultiplier with position capability

"Valeu a pena? Tudo vale a pena
Se a alma não é pequena."

— F.P.

Universidade de Aveiro Departamento de Física
2013

Tiago
Neves Lopes

Fotomultiplicador gasoso sensível ao UVV com resolução em posição

VUV single photon Gas Photomultiplier with position capability

Dissertação apresentada à Universidade de Aveiro para cumprimento dos requisitos necessários à obtenção do grau de Mestre em Mestrado Integrado em Engenharia Física, realizada sob a orientação científica do Doutor João Filipe Calapez de Albuquerque Veloso, Professor Auxiliar do Departamento de Física da Universidade de Aveiro

Apoio financeiro aos projectos: PTDC/FIS/110925/2009, "Desenvolvimento de foto-detectores para leitura em detectores RICH" e PTDC/FIS/110937/2009, "Fotomultiplicador gasoso com fotocátodo de bialkali para a região do visível e com resolução de posição

Dedico este trabalho à minha família e aos meus amigos, por tudo o que são e representam na minha vida.

o júri / the jury

presidente / president	Professora Doutora Teresa Maria Fernandes Rodrigues Cabral Monteiro Professora Associada, Departamento de Física da Universidade de Aveiro
vogais / examiners committee	Doutor Fernando Domingues Amaro Investigador, Centro de Instrumentação do Departamento de Física da Universidade de Coimbra
	Professor Doutor João Filipe Calapez De Albuquerque Veloso Professor Auxiliar, Departamento de Física da Universidade de Aveiro

agradecimentos /
acknowledgements

Agradeço:

- Aos meus pais, à minha família e à minha namorada a paciência e o apoio dado em todos os momentos
- À Guida a capacidade de me fazer ver a vida sobre uma outra perspectiva e ter sido uma âncora em todo o meu curso
- Aos membros do DRIM, que foram pessoas fantásticas e me ajudaram a crescer como Engenheiro Físico durante o meu percurso académico e pela boa disposição e espírito colectivo demonstrado. Um especial agradecimento ao Carlos, à Ana e à Lara.
- Ao Professor João Veloso, por todas as oportunidades que me proporcionou e pelo facto de me ter aberto a porta à 3 anos atrás quando já estava cheio de gente no laboratório
- À Universidade de Aveiro, em especial aos docentes do Departamento de Física por terem transmitido os seus conhecimentos e terem ajudado na minha formação profissional
- Por fim, agradeço a todos aqueles que me foram pondo barreiras e descrença, já que me fizeram superar e ser melhor

A todos, de coração, o meu muitíssimo OBRIGADO.

Palavras Chave

Detectores gasosos em micropadrão, detecção de fotões UV, fotocátodos sólidos, Imagiologia em Detectores gasosos, 2D-THCOBRA, Fotomultiplicador Gasoso

Resumo

O presente trabalho baseia-se no desenvolvimento e estudo de um fotomultiplicador gasoso na região do Utra-Violeta de Vazio (UVV) e com capacidade de discriminação de posição. O detector é constituído por duas THGEM seguidas de uma 2D-THCOBRA, a operar em Ne/CH4(5%) à pressão de 1 bar e em modo de fotão único.

A 2D-THCOBRA é uma estrutura híbrida, que resulta da combinação entre uma THGEM e uma 2D-MHSP, beneficiando da robustez e resistência às descargas da primeira e dos dois estágios de multiplicação e da capacidade de discriminação da posição da 2D-MHSP.

Neste trabalho foi estudada a influência dos potenciais aplicados aos eléctrodos da 2D-THCOBRA no ganho e no refluxo de iões (IBF) do detector. Foi ainda avaliada a resolução em posição deste detector.

Foram medidos ganhos da ordem de 10^6 e, para estes valores de ganho, IBF na ordem dos 20%. Obteve-se ainda resoluções em posição inferiores a 300 μm.

Keywords Micropattern gaseous detectors, Photon detectors for UV, solid-photocathode, gaseous imaging detectors, 2D-THCOBRA, Gas Photomultiplier

Abstract A new position sensitive gas photomultiplier for the Vacuum Ultraviolet (VUV) region is presented in this work. The detector is composed by two THGEMs, followed by a 2D-THCOBRA being operated in Ne/CH4(5%), at 1 bar pressure in single photon mode.
The 2D-THCOBRA is an hybrid microstructure which combines the robustness and the resistance to discharges of a THGEM with the two independent charge multiplication stages and the position discrimination of the 2D-MHSP.
In this work the 2D-THCOBRA influence in the charge gain and IBF values was studied. The position resolution of the entire system was also studied.
The achieved results shown a charge gain of 10^6 and, for this gain values, an IBF value of about 20%. Position resolutions below 300 μm were also obtained.

Publications and Communications in the context of this thesis

Papers in international scientific periodicals with referees

- C.D.R. Azevedo,F.A. Pereira, **T. Lopes**, P. Correia, A.L.M. Silva, L.F.N.D. Carramate, J.F.C.A. Veloso; *"A Gaseous Compton Camera using a 2D sensitive gaseous photomultiplier for Nuclear Medical Imaging"* Nuclear instruments and Methods A (2013), in press, http://dx.doi.org/10.1016/j.nima.2013.05.116

- A.L.M. Silva, C.D.R. Azevedo, L. F. N. D. Carramate, **T. Lopes**, I.F. Castro, R. de Oliveira, J.F.C.A. Veloso *"X-ray Imaging Detector Based on a Position Sensitive THCOBRA with Resistive Line"* Journal of Instrumentation 8 (2013) P05016

- **T. Lopes**, A.L.M. Silva, C.D.R. Azevedo, L.F.N.D. Carramate, D.S. Covita, J.F.C.A. Veloso *"Position sensitive VUV gaseous photomultiplier based on Thick-multipliers with resistive line readout"* submitted - Journal of Instrumentation (Junho de 2013)

International conference with referees

- C. A. Santos, F. Pereira, **T. Lopes**, C. D. R. Azevedo, F. D. Amaro, J. M. F. Dos Santos, A. Breskin, R. Chechik, J. F. C. A. Veloso; *"Ion Back Flow Reduction Using a THCOBRA in a THGEM Based VUV Photosensor"* (Poster) - IEEE 2012 Nuclear Science Symposium and Medical Imaging Conference, October 29 - November 3, 2012, Anaheim, California, USA

- A.L.M.Silva, C.D.R. Azevedo, L. Carramate, **T. Lopes**, R. de Oliveira, J.F.C. Veloso; *"X-ray imaging detector based on a 2D sensitive THCOBRA with resistive line readout"* (Talk/Poster) - IEEE 2012 Nuclear Science Symposium and Medical Imaging Conference, October 29 - November 3, 2012, Anaheim, California, USA

- J.F.C.A. Veloso, C. D. R. Azevedo, F. Pereira, **T. Lopes**, P. Correia, A. L. M. Silva and L. F. N. D. Carramate; *"A Gaseous Compton Camera using a 2D sensitive gaseous phtotomultiplier for Nuclear Medical Imaging"* (poster)13th Vienna Conference on Instrumentation (VCI), Vienna, Austria, 11-15 February, 2013

- **T. Lopes**, C.D.R. Azevedo, A.L.M. Silva, D.S. Covita, F.A. Pereira, C.A. Santos, J.F.C.A. Veloso; *"VUV sensitive gaseous photomultiplier with position capability based*

on thick multiplier" MPGD 2013 - 3rd Conference on Micro-Pattern Gaseous Detectors, Zaragoza, Spain, July 1-4, 2013.

- C.D.R. Azevedo, F.A. Pereira, **T. Lopes**, P. Correia, A.L.M. Silva, L.F.N.D. Carramate, J.F.C.A. Veloso; *"A Gaseous Compton Camera with MPGD-based readout"* MPGD 2013 - 3rd Conference on Micro-Pattern Gaseous Detectors, Zaragoza, Spain, July 1-4, 2013.
- A.L.M.Silva, C.D.R. Azevedo, L. Carramate, **T. Lopes**, J.F.C. Veloso; *"Further studies on the position-sensitive THCOBRA for imaging purposes"* MPGD 2013 - 3rd Conference on Micro-Pattern Gaseous Detectors, Zaragoza, Spain, July 1-4, 2013.

Contents

List of Figures

List of Tables

Introduction

Although always present in the man's history, the ionizing radiation has only be discovered about 100 years ago. The first reports of a non-visible radiation date from 1895, when Rontgen saw the luminescent screen shows a green light provided by a Hittorf-Crooks tube, which was covered with a black shield. Rontgen also discovered that the "new radiation", which he named X-rays, was able to make the air an electrical conductor [1].

These discoveries promote a demand of materials and instruments that were capable to detect the radiation. Since the air could act as an electrical conductor, and the charges generated by radiation can easily be moved under the influence of an electric field, some detectors using gas as detection medium were created in the following years - usually called as ionization chambers[1].

However, was, in 1928, with the introduction of the Geiger-Müller Counter that the gas-filled detectors exploited being the first detector capable to respond to individual radiation events. This detector uses the so called "gas multiplication", which is achieved by applying an high electric field that accelerates the electrons promoting the ionization of the gas. This process corresponds to an avalanche amplification of charges, named "Townsend avalanche" [2].

In the late 1940s, the proportional counter was introduced also based in the principle of the charges multiplication in a gas medium, however, using lower values of electric field. This allows that each original electron leads to an avalanche,where the charge collected is proportional to the number of original electrons, allowing to apply this detectors no only as a counter but also in applications that needs energy information like as spectroscopy. In other way the proportional counters need external amplification, since the number of electrons collected by this detector is not sufficient to read the signal directly.

In the following years new gas detectors were introduced. A very famous one in particle physics was responsible for the attribution of a Nobel Prize in Physics to George Charpak in 1992, the Multiwire Porportional Chamber [3]. However, the next big step in this field was the introduction of the Micropattern Gas Detectors (MPGDs), which happened due to the developments in micro-lithography techniques. The first MPGD was introduced by Microstrip Gas Chamber (MSGC) [4], followed by Gas Electron Multiplier(GEM)[5] and later bt MICRO MEsh GAseous Structures (MICROMEGAS) [6]. On the last years several hibrid micropatterned devices have appeared as for example, the MicroHole Strip Plate (MHSP)[7], a microstructure resulting of the combination of a GEM and a MSP [8].

The common properties of the MPGDs are the high gain, the good position resolution with energy discrimination combined with the low cost and the large-area capability. Beside

this characteristics, the MPGDs still have the ability to be compatible with magnetic fields, make them unique comparative with the solid state detectors [8]. Thus, recently, several experiments have been equipped with MPGDs like Totem [9] or committed to the detectors upgrade with such technology as for instance COMPASS [10] or ALICE [11], etc.

Following the success of the described detectors and based on their operation principle, the so called Thick-Structures were introduced, fulfilling the need of robustness and stability of the existing detectors. The most spread device is the THick-GEM (THGEM) [12]: a GEM like structure, where the Kapton substrate was replaced by regular Printed Board Circuit (PCB) substrate. Another structures, recently, introduced was the THCOBRA [13], an hybrid structure that benefits of the robustness and stability of the THGEM and the two multiplication stages that characterizes the MHSP.

State of Art

This work is based on study and development of a VUV single photon ($\lambda \leq 200$ nm) Gas PhotoMultiplier (GPM) with a position discrimination capability. In general the gaseous photomultipliers are capable to cover a large-area and to obtain high gains values allowing an efficient detection at single-photon levels. In particular this GPM can be used in different fields of radiation detection ranging from applications in medical imaging (the same structures could be used Gaseous Compton Camera [14]) to particle physics - for example as RICH detector.

A critical element of the GPMs is the photocathode, which is responsible for the detection of the photon through the emission of electrons. Several types of photocathodes can be used: gaseous photocathodes, as a TEA (triethylamine) or TMAE (tetrakis-dimethylamine-ethylene), or solid photocathodes, being the CsI (Cesium Iodide) the most used material for the detection of VUV photons and presenting the highest quantum efficiency among all the existing solid photocathodes.

GPMs still presenting some limitations as the Ion Back Flow (IBF) and ion-induced secundary-electron emission. In this way, the MPGDs, especially GEM and MHSP, assume a important role to reduce this effects, due to the fact that they are multipliers of closed geometry - the amplification of charges occurs within a specific volume - and they can be placed in cascade configuration, allowing higher gains and intrinsically an IBF reduction.

Besides the good results obtained with GEM's and MHSP's, especially when in cascade configuration, there was the need to give the GPM some robustness and sparks resistance. Thus, some studies involving the thick structures were in course [15].

Some results using the thick-structures have shown an higher gain when compared to the thin-structures, however show larger values of IBF [15]. Recent studies using Flipped-Reverse-THCOBRA (the cathode and anode strips of the THCOBRA are at the top and both electrodes changed - the cathode electrode is the central electrode) were performed. Values of about 5% were obtained, which open a good prospects to further reduce the IBF [16].

In this works we will present results on the study of the main characteristics, as Gain, IBF and position resolution for a GPM using two THGEM and a THCOBRA.

In order to obtain image capability a simple resistive readout was implemented in the THCOBRA, here named as 2D-THCOBRA. This device have shown position resolution in order of 2,3 mm, for 8 keVs X-rays, in Ne/5%CH4 [17].

CHAPTER 1

Radiation Gaseous Detectors

1.1 Physical Principles

The presented thesis focus on the detection of the VUV photons using gaseous detectors, thus to understand the work is necessary to know the fundaments of the interaction of radiation with matter.

1.1.1 Interaction of Radiation with Matter

The main interactions associated the radiation with matter are: pairs production (and annihilation), Compton Scattering and Photoelectric Absorption. All these processes are characterized by the energy transfer from the photon energy to electron energy [2]. As in this work the used radiation was the VUV photons ($\lambda \leq 220$nm, approximately) the main process of the mentioned phenomena is the Photoelectric Absorption.

1.1.1.1 Photoelectric Absorption

The Photoelectric Absorption process is characterized by an interaction between a photon and an absorber, where the energy of the photon causes the extraction of an electron, called *photoelectron*, with the absorption of the photon.

The Photoelectric Absorption process can be divided into a several steps: the first step corresponds to the transfer of the photon energy to an electron of the medium; the second one is related with the electron-electron collisions and the loss of the energy during the migration to the surface; and the last step is the minimum electron energy needed to overcome the potential barrier. The minimum energy transferred to the electron that can allow the extraction of the photoelectron from the material is called the *Work Function* [2]. When the photon energy is higher than the work function, the remaining photon energy is transferred to the photoelectron, in term of kinetic energy as presented in the following equation (1.1):

$$E_c = h\nu - \phi \tag{1.1}$$

where E_c is the photoelectron Kinetic Energy, ϕ is the work function and $h\nu$ is the energy of the incident photon.

The interaction between the photon and the material, also creates an ionized atom (due to the loss of one electron) which returns to original electronic configuration through capture of a free electron from the medium and/or due to the rearrangement of electrons.

1.1.1.2 Photocathode

As already mentioned the photocathode is a photo-converter, that can eject an electron when receiving a stimulus from a photon, being explained by the photoelectric absorption process. Generally a solid photocathode is built from thin films of different materials, usually *alkali metals* with very low work functions, maximizing the number of ejected electrons per incident photon.

Photocathodes can be classified according to their geometry as: reflective photocathode or semi-transparent photocathode, both schematically shown in figure 1.1. In a reflective geometry, the photoelectron is ejected from the same surface of photon interaction - figure 1.1(a). In the semi-transparent geometry the photoelectron is ejected from the opposite surface of the photon interaction demanding a thinner photocathode. In semi-transparent geometry, the photocathode is generally deposited on the detector window - figure 1.1(b).

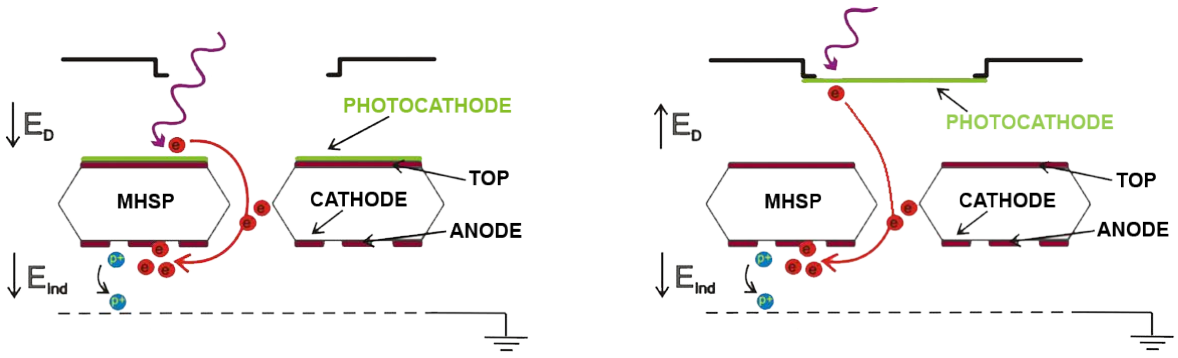

(a) (b)

FIGURE 1.1: **Schematic drawing of Photocathode Geometries: a) Reflective Geometry; b) Semi-transparent Geometry.**

However, not always a photon interacts with the photocathode leads to a photoelectron ejection. The probability of a successful photoelectron extraction per impinging photon is denominated *Quantum Efficiency* (QE), mathematically represented by the expression (1.2):

$$QE = \frac{N_{pe}}{N_{ph}} \tag{1.2}$$

where N_{pe} is the number of ejected photoelectrons and N_{ph} is the number of photons that reach the photocathode. The QE depends of different parameters as the photocathode material, photocathode geometry, substrate material, the deposition technique or atmosphere exposure conditions and the incident photon wavelength [18, 19].

In figure 1.2 the QE is shown as a function of the wavelength (λ) for several photocathodes.

From the figure it is clear that the CsI photocathode, in reflective geometry, is the one which presents the higher value of QE with a cut-off near to 220 nm. Beside these characteristics the CsI photocathodes presents other advantages, like: easiness of preparation, the deposition is done by standard thermal evaporation technique [18]; it is able to cover a large area and can operate in high radiation flux under high multiplication conditions, due to the low volume and high resistivity.

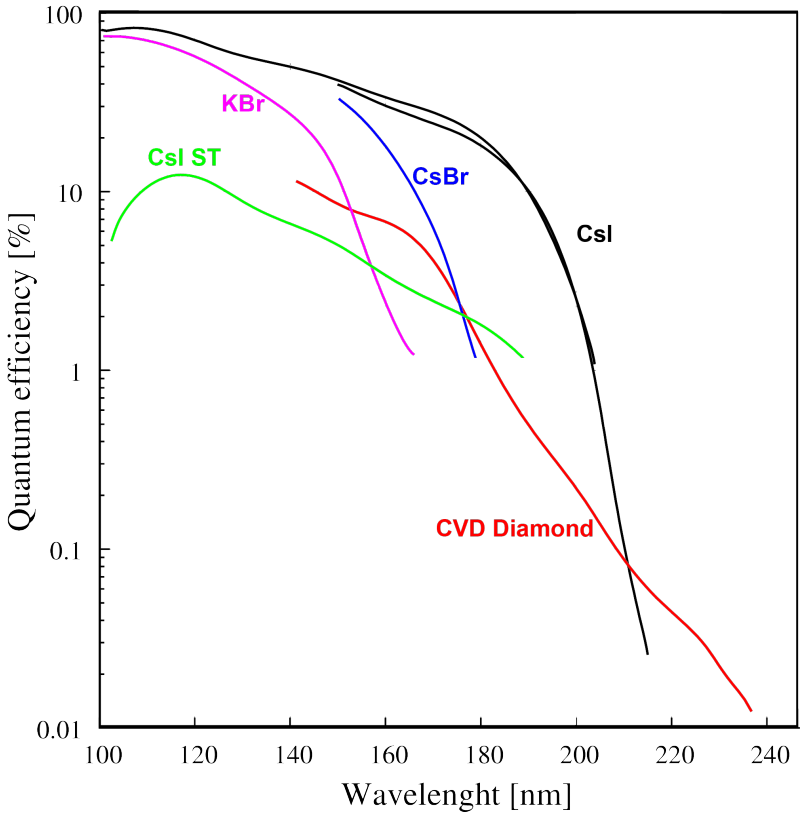

FIGURE 1.2: **Photocathode *QE* curves for different material, adapted from [20, 19].**

Those are also the reasons that triggered, in this work, the choice of a CsI reflective photocathode.

1.2 The Gas-Filled Detectors

On a gas-filled detector when a electric field is present, the charges created by the incident radiation are separated, drifting to the respective electrodes, anodes or cathodes. The figure 1.3 shows the variation of the charge collected with the increase of the electric field.

If the electric field is low, a loss of electron energy and consecutively, recombination can occur due to the successively collisions between electrons and gas atoms/molecules. By increasing the electric field, the probability of each formed pair migrate to respective electrode also increases, whereas for a particular electric field value all the formed charges reach their electrode. This behavior (**Ion Saturation Region**) continues until the value of the electric field is such that the accelerated charges have enough energy to promote the ionization of the gas atoms/molecules. The resulting charges of the second ionization are accelerated and can promote successively other ionization, causing an avalanche in charge, called *Townsend Avalanche*. This exponential increase of charges lead to a number of charges created is proportional to the number of primary charge (**Proportional Region**).

When the charge amplification is too high, due to the continuous increase of the electric field, the positive ions can distort the electric field locally, and therefore the number of ions-pair formed decrease, ending the Proportional Region. In this region, **Geiger-Müller Region**, the number of electrons presents in the avalanche are bigger than the other regions creating a several avalanches in the detector medium, which stops due to the amount of ions produced during this process,i.e., is self contained. However the number of produced electrons

in this regime are not proportional to the deposited energy.

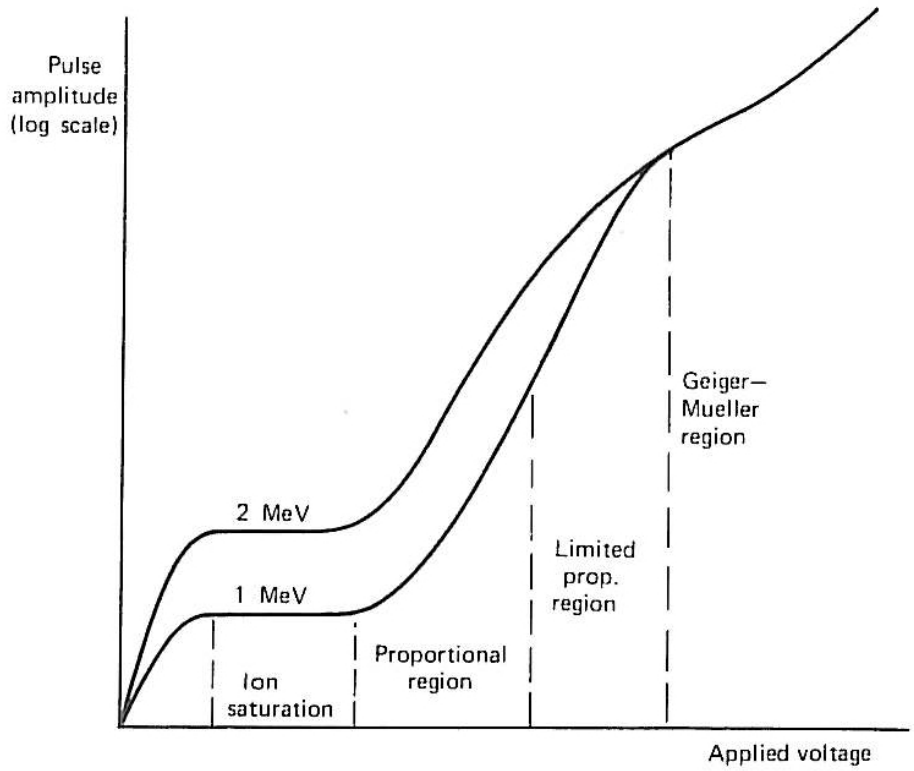

FIGURE 1.3: **The regions of operation of Gas Filled Detectors [2]**

1.2.1 MPGD's: Micropattern Gas Detectors

Despite the success of the Multi-Wire Proportional Chamber (MWPC) [3], yielded the Nobel Prize for its autor, Georges Charpak, there was need to develop detectors which were able to operate at high counting rates with good energy resolutions and imaging capability. These conditions impose that the "'new detectors" presents a short distance between the electrodes (in order to have a high counting rate) and a large area. Thus appeared the new gaseous detectors, the Micropattern Gas Detectors.

1.2.1.1 The Microstrip Plate (MSP)

The Microstip Plate, proposed, in 1988, by A.Oed [4] was the first step in the MPGD's age. It consist on a pattern of strips with different widths, as represented in figure 1.4(a). The thinner ones, with 10 μm, are the anodes while the thicker strips represent the cathode electrode, which present typical width values ranging from 60 till 100 μm. These metal strips are printed onto an insulator substrate using a photolithographic and etching techniques.

The charge amplification in MSP is produced in the anodes vicinity due to the high voltage difference between the electrodes, being the electrons rapidly collected in anode strips while the ions drift for the cathodes, quickly. This short collection time is an advantage of this gaseous detector, allowing to have a high rate operation.

The imaging capability is achieved by structuring the bottom side of this structure in strips orthogonally positioned relatively to the anodes strips - as illustrated in figure 1.4(b), being the signal induced from the collection of the electrons in the anodes.

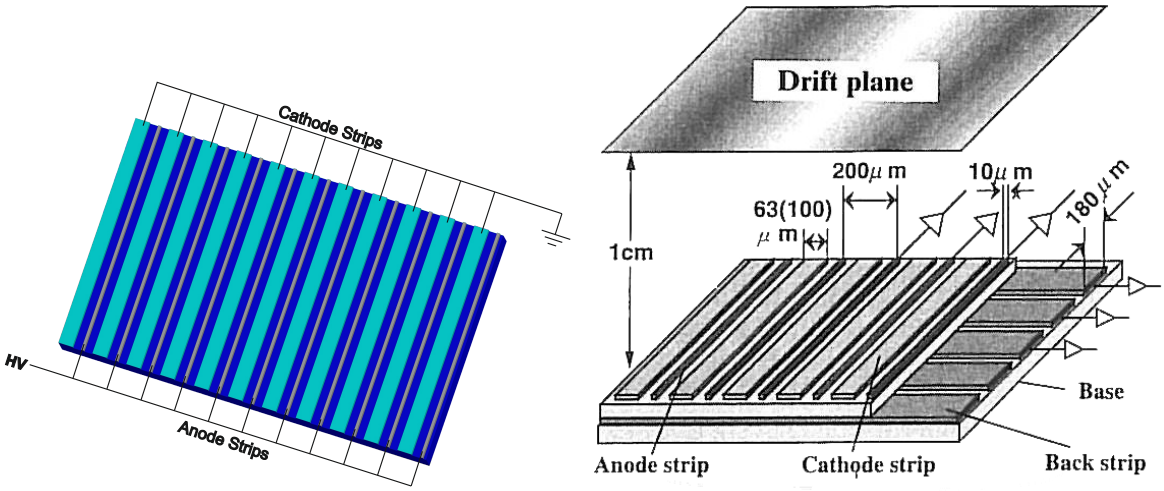

(a) (b)

FIGURE 1.4: **1.4(a) Schematic drawing of a Microstrip Plate;1.4(b) Structure of a two-dimensional position-sensing MicroStrip Gas Chamber, adapted from [2]**

The small distance between the electrodes and their small width, which allows high rate operation, presents drawback as it makes the detector sensitive to discharges, causing physical damages or even destruction of the electrodes.

1.2.1.2 The Gas Electron Multiplier (GEM)

The Gas Electron Multiplier is made from a thin Kapton foil (50 μm thick) with a 5 μm copper cladded layer on both sides [5]. A hexagonal pattern of holes (typically a diameter of 60-70 μm) is etched with a 140 μm. Applying a suitable voltage difference between the electrodes, a strong electric field is generated inside the holes and thus leading to electron multiplication.

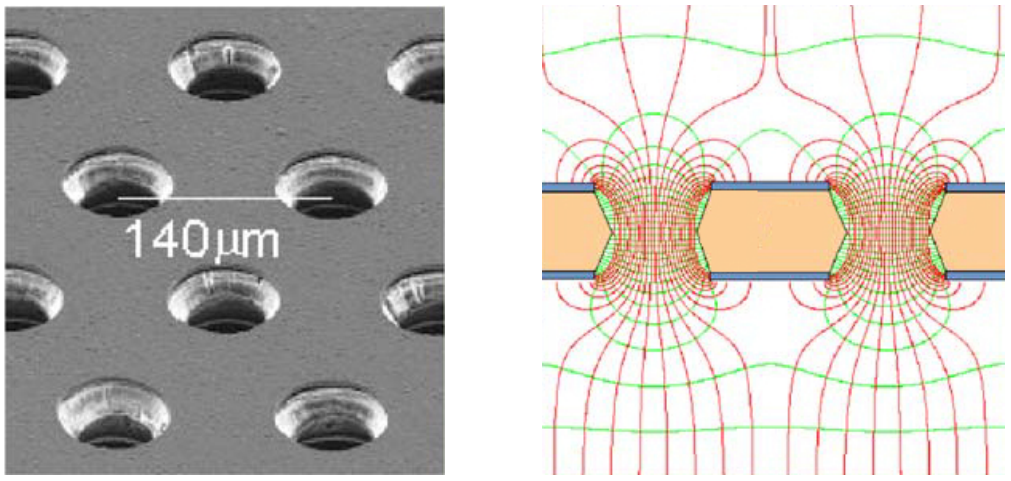

(a) (b)

FIGURE 1.5: **1.5(a) Photography of a typical GEM [21];1.5(b) Schematic drawing of the operation principle of a GEM, with the electric field lines, adapted from [21].**

As the electrons are able to cross the structure, it is also possible to have a cascade configuration where the electrons undergo on multi-stage gas amplification. This configuration allows higher gain, decreasing the discharge probability by reducing the voltage across the GEM holes. The cascade configuration also reduces the Ion Back Flow due to the ion trap in the electrodes. Low IBF is essential for photodetectores using photocathode [15].

1.2.1.3 The Micro Hole Strip Plate (MHSP)

The Micro Hole Strip Plate (MHSP) is an hybrid MPGD resulted from the combination of the two referred structures above (GEM and MSP). Thus the MHSP consists in a GEM like structure where one side is structured into strips, as can be seen in figure 1.6(a). The strip that surround the holes, the wider strips, represents the cathode electrode while the anode electrodes are the narrower strips, like in MSP. This design allows the MHSP to have in a single structure two multiplication stages, the first one similar to the GEM - multiplication within the holes - and a second one similar to MSP, which occurs in anode vicinity, as illustrated in figure 1.6(b).

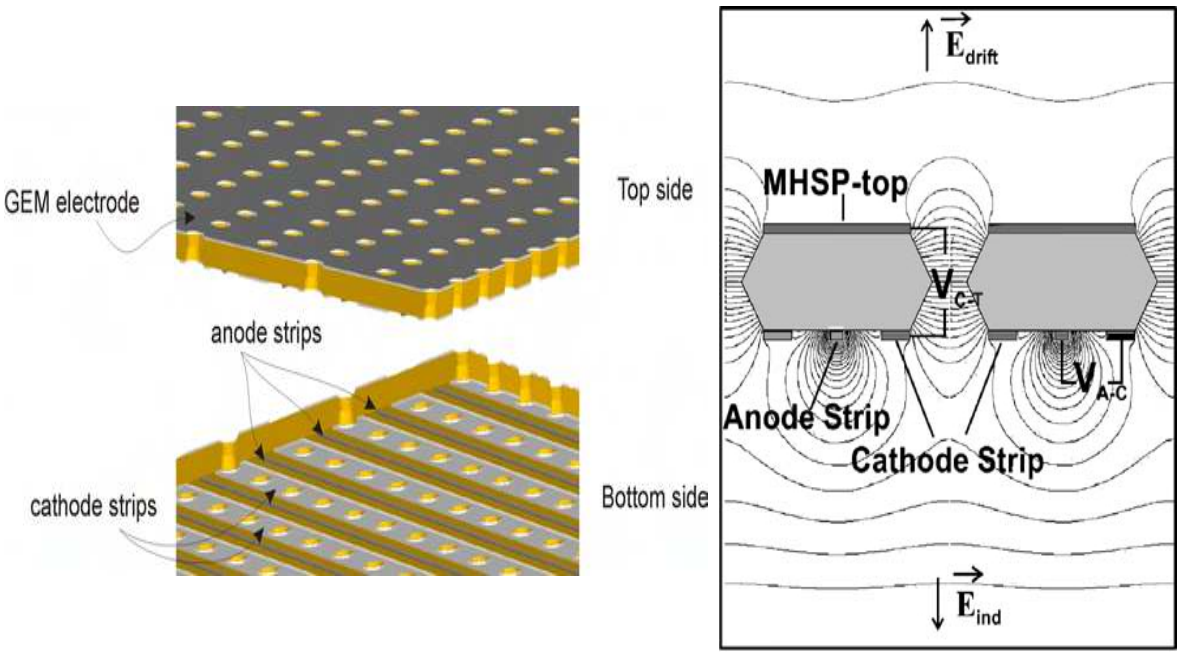

(a) (b)

FIGURE 1.6: **1.6(a) Schematic drawing of a MicroHole Strip Plate [22]; refMHSP:fig2 Schematic drawing of the operation principle of a MHSP, with the electric field lines, adapted from [23]**

Due to the two multiplications stages this structure presents a higher gain when compared to a single-GEM or to MSP [23]. It also presents a higher reduction of the ion-back flow, since some ions are trapped at the cathode electrode [24] . It has imaging capability, if the top side is structured into orthogonal strips relatively to the anodes strips. In this case the MHSP is denominated as 2D-MHSP.[25].

1.2.1.4 The Thick-GEM (THGEM)

Despite the success achieved by the structures mentioned above, they present some constrains such as the high sensitivity to discharges, that could lead to the destruction, or the

straightness at very large areas.

This fact triggered the development of the *Thick*-structures, which more robust, more resistant to electrical discharges and can be applied to large areas without having to be stretched.

In particular, one of the *Thick*-structures is the *Thick*-GEM (THGEM). As its name indicates, this structure is based on GEM, although with a different substrate material, a standard PCB (400 - 800 μm thickness) with the holes mechanically drilled. The rim, a small ring etched around the holes gives a greater stability to the structure, since the probability of discharge is reduced, and therefore allowing higher gains [26].

The standard THGEM presents holes with a diameters ranging from 300 to 1000 μm distributed in hexagonal pattern (700 - 1300 μm) and with a 0-100 μm rim chemical etched, as illustrated in figure 1.7 [27].

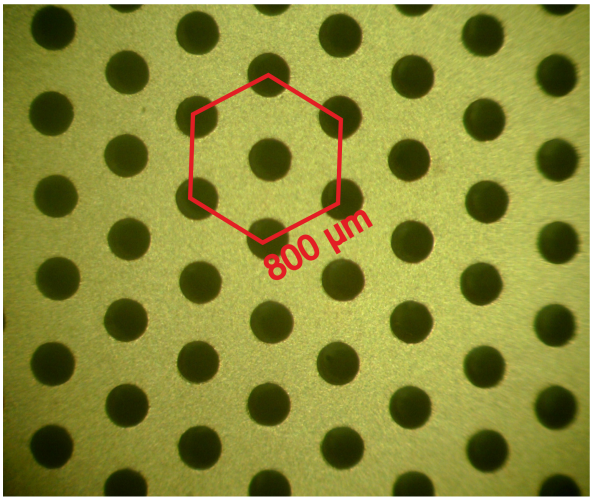

FIGURE 1.7: **Photography of the first THGEM of the detector used in this work. It has a pitch of 800 μm, 400 μm of a hole diameter and no rim.**

Similarly to what happens with the GEM, the THGEMs can also be placed in a cascade configuration, benefiting from the same properties, or in other words a higher total gain with reduced discharge probability and an intrinsic ion back flow reduction.

1.2.1.5 The Thick-COBRA (THCOBRA)

The THCOBRA is a combination of the THGEM with a MHSP, exploiting the main characteristics of each one. This structure have the robustness and the low cost characteristics of the THGEM and the two stages of multiplication, the position discrimination and the ion blocking capability of the MHSP [28].

In this way, the THCOBRA consists in a PCB mechanical drilled, with the same parameters of the THGEM. In one side of this structure a strip pattern is etched, being the cathodes electrodes surrounding the holes and the anodes strips running through the space between the cathodes. The name of this structure comes from the similarity between the holes and anode strips pattern with the movement of a snake ("Cobra"). The top and the bottom side of THCOBRA are presented in figure 1.8.

The operation principle of this structure, as illustrated in figure 1.9, is similar to the MHSP since the first multiplication occurs inside the holes and the second occurring in the anode vicinity. During this work we will be refer V_{CT} to the voltage difference between the

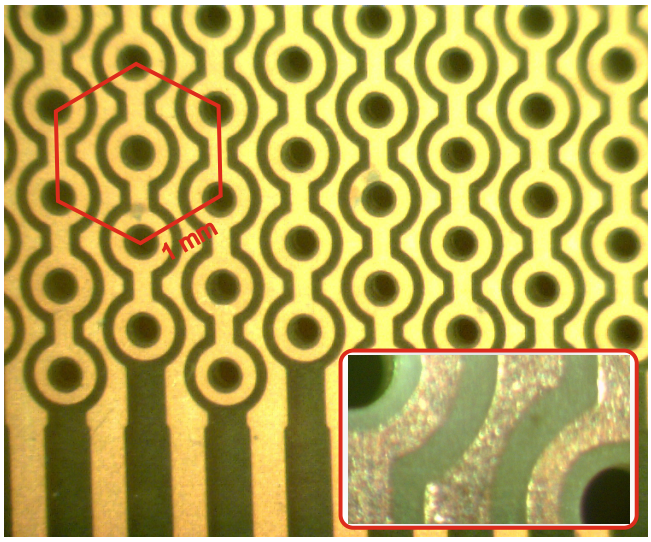

FIGURE 1.8: **Photography of the THCOBRA used in this work. In detail, the unit cell of the THCOBRA, showing the rim presence.**

cathode and the top electrodes and V_{AC} for the voltage difference applied between anode and cathode strips.

For imaging proposes this structure can also be structured in a similar way as the MHSP, with the top electrode presenting orthogonal strips relatively to the anode strips. In this case the structure is called by 2D-THCOBRA. The present work will show some characteristics of this structure when used to detect VUV photons and produced an image.

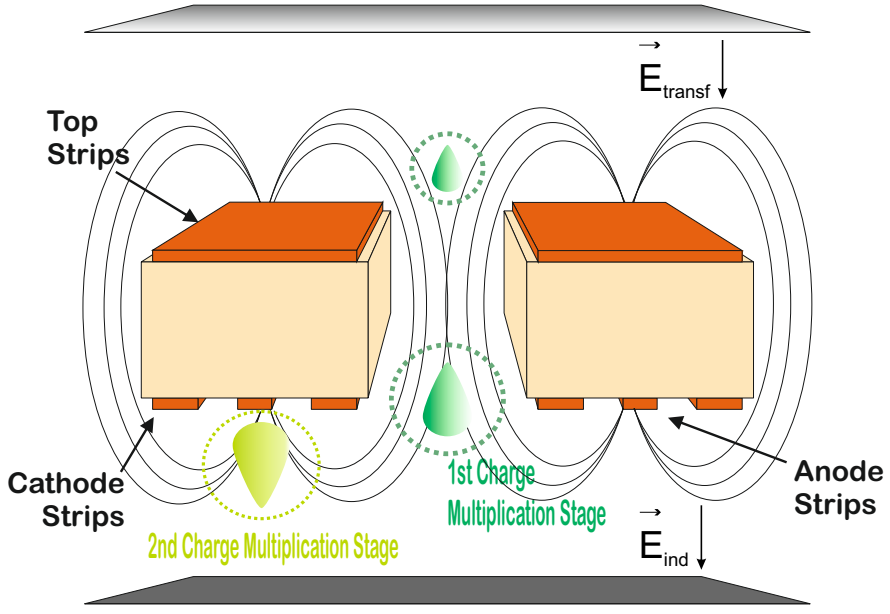

FIGURE 1.9: **Schematic drawing of the operation principle of the THCOBRA. It presents two stages of multiplication: one inside the holes and another in the anode vicinity, being the final charge collected in the anode strips.**

CHAPTER 2

The Experimental Setup

2.1 Detector Configuration

The detector used in this work is composed by three structures arranged in a cascaded configuration. The first two structures are THGEMs while the last one is a 2D-THCOBRA, being equally distanced by 3 mm as shown in Figure 2.1.

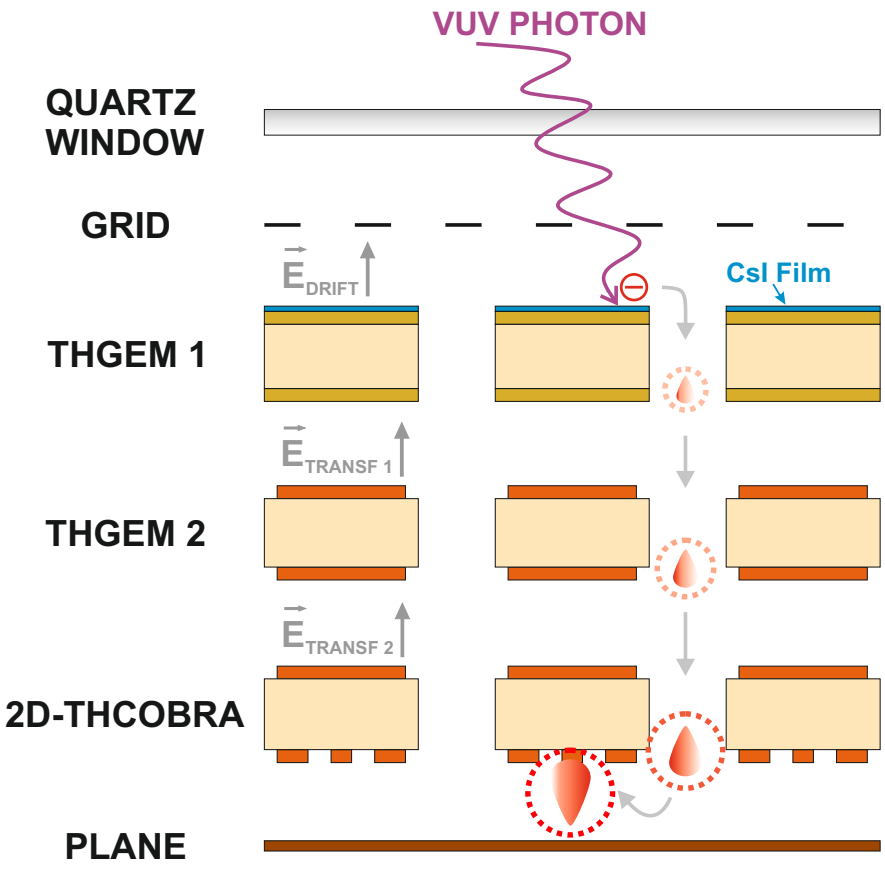

FIGURE 2.1: **Schematic drawing of the detector configuration and his operation**

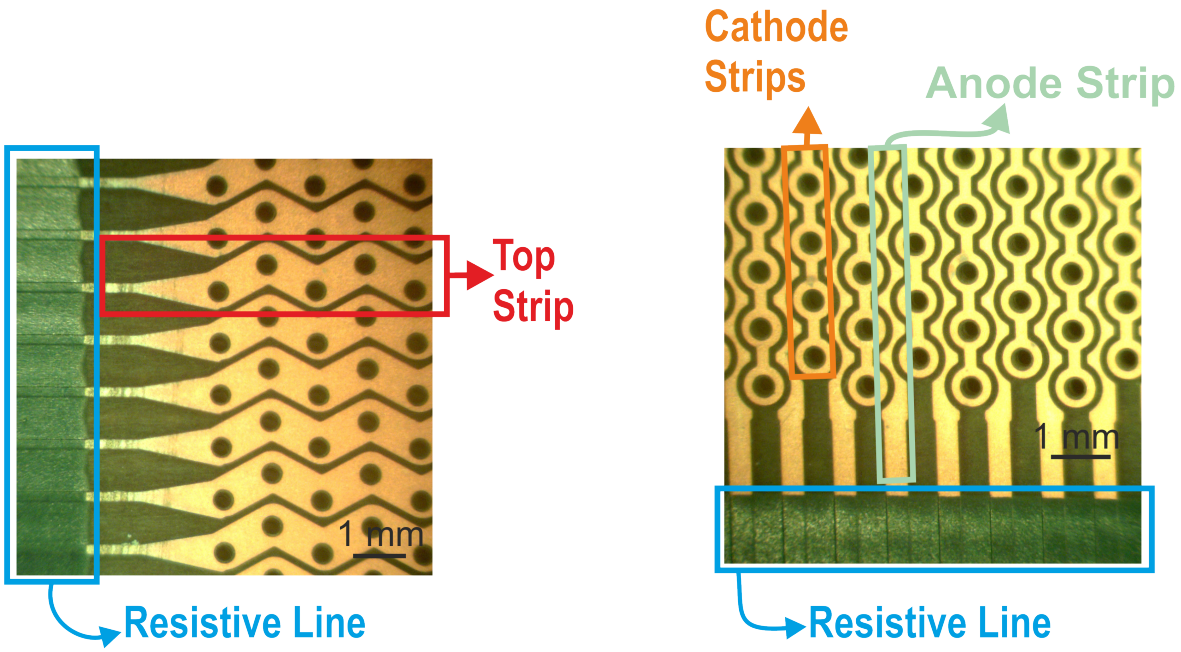

(a) (b)

FIGURE 2.2: **Detailed view of the 2D-THCOBRA: 2.2(a) top side and 2.2(b) bottom side**

In particular, the 2D-THCOBRA, shown in Figure 2.2, also presents strips etched by photolithography process, with width of 200 μm. The 2D-THOCOBRA presents the top and anode strips orthogonally disposed in order to obtain the two dimensions of an image. At the end of the anode and top strips a resistive line is deposited, through serigraphy process, with approximately 15 kΩ. Here, in the resistive lines, occurs the charge division. By reading the charge signal at each end of the resistive lines the particle interaction position can be found by applying simple center of mass like methods - detailed described in section 2.3.3.1. As illustrated, the 2D-THCOBRA also presents a rim in both sides of the structure. The other characteristics of the 2D-THCOBRA are presented in 2.1.

In table 2.1 is summarized the geometric details of the structures used in this detector.

TABLE 2.1: **Used Structures: Specifications**

Structure	Pitch (μm)	Hole Diameter (μm)	Rim (μm)
THGEM 1	800	400	-
THGEM 2	1300	700	100
2D-THCOBRA	1000	400	80

On the top of the first structure (THGEM 1), a CsI photocathode was deposited by thermal deposition, in order to cover the entire sensitive area, i.e. a square area of 35x35 mm^2.

In addition to the three structures, the detector also presents: a 5 mm thickness quartz window (spectrosil B), which allows the VUV photons to reach the photocathode without being absorbed by the window material [29], figure 2.3. The drift region, between the stainless grid and the top of the first THGEM (THGEM1), was set to 3 mm. The induction region, delimited by the copper plate (Plane) an the bottom of the 2D-THCOBRA, was polarized at the same potential of the 2D-THCOBRA cathode.

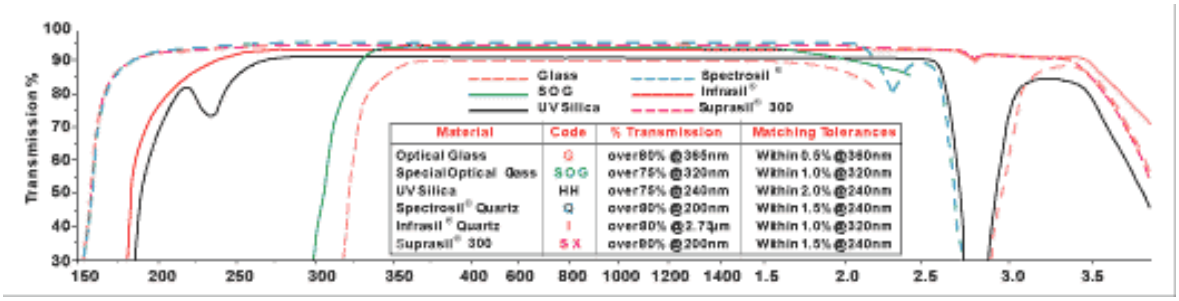

FIGURE 2.3: **Transmission curves of the Spectrosil B quartz window [29].**

The VUV photons were provided by a Hg(Ar) lamp - NewPort 6035 Spectral Calibration Lamp, having three main lines in the photocathode sensitivity region: 185, 187 e 194 nm [30].

Some acronyms are used to simplify the reference of the different parts of the detector. The figure 2.4(a) show the relation between this and the different structures of the detector.

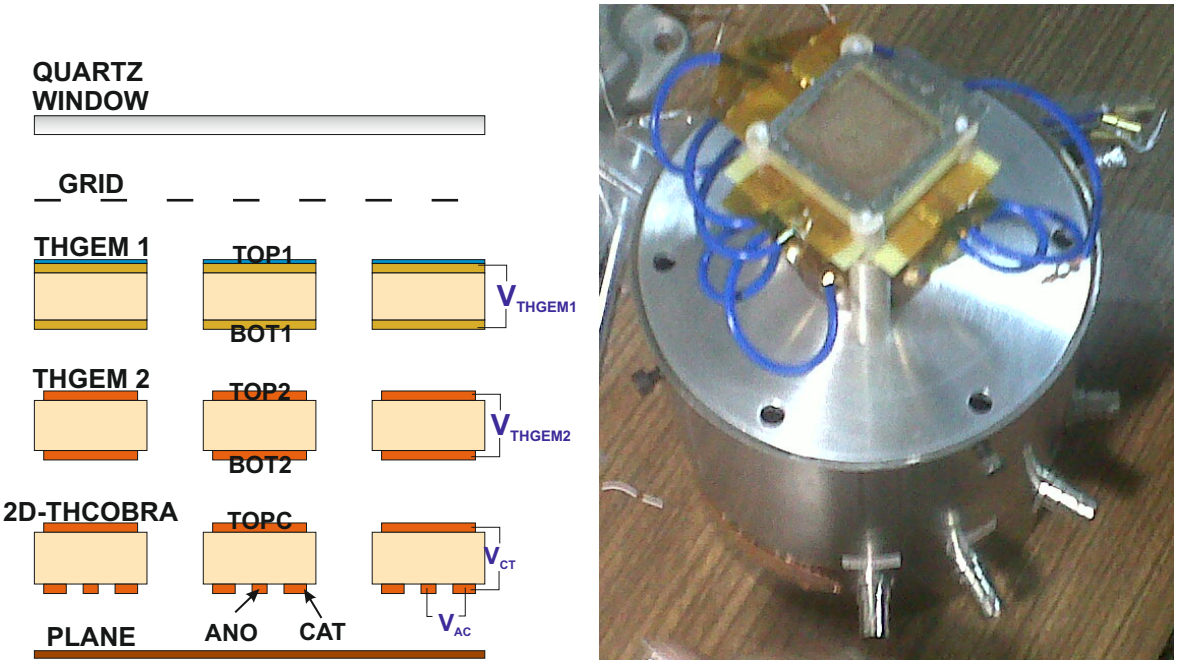

(a) (b)

FIGURE 2.4: **2.4(a) Schematic drawing of the detector configuration and used names to refer the different structures of the detector; 2.4(b) A photo of the detector used in this work**

Operation Principle

The detector operation principle is, also, shown in Figure 2.1. When the VUV photon impinges the CsI photocathode an electron can be ejected into the gas medium, through photoelectric effect, being denominated as photoelectron. If a suitable electric field is applied in the drift region or/and inside the holes of the THGEM1, the photoelectron drifts towards the THGEM1 holes, where the first charge multiplication stage occurs. After the first charge multiplication stage, the emerging charge is transferred into the THGEM2, where a second multiplication charges occurs - similar to the first one. The resulting charge is finally drifted

to the 2D-THCOBRA. This drift and focusing of electrons inside the detector is only possible if successive and suitable potential differences are applied between the electrodes of the structures.

When the charges enter on the 2D-THCOBRA holes another Townsend avalanche occurs. If a suitable V_{AC} is set, a second multiplication occurs, being the final charge collected in anodes electrodes.

The charges collected in the anode strips induce a signal in the top electrodes. This two signal, in the top and anode electrodes, are divided in each resistive line, originating four signals which are used to determinate the interaction position of the VUV photon and detector amplitude response.

2.2 Operation Modes

For each photon that interacts with the photocathode and can release a photoelectron, which could originate an avalanche process, two different operation modes are used: *pulse mode* and *current mode*. These different modes are used for different type of measurements.

2.2.1 Current Mode

In current mode the information is accessed by the integration of the produced charge ($I(t)$) from a set of pulses within a time window - figure 2.5(a). Although this mode discards the most pulse fluctuations, since is based on charge averaging. There are always some variations, due to the statistical uncertainties in the signal produced by the electronic noise, that make oscillations on the $I(t)$ value around a fixed point (I_0) - figure 2.5(b). Due to these fluctuations is necessary to guarantee that the range (r) of the radiation current is high enough, when compared with the produced current from electrical noise, to allow a high signal to noise ration and a precise measurement.

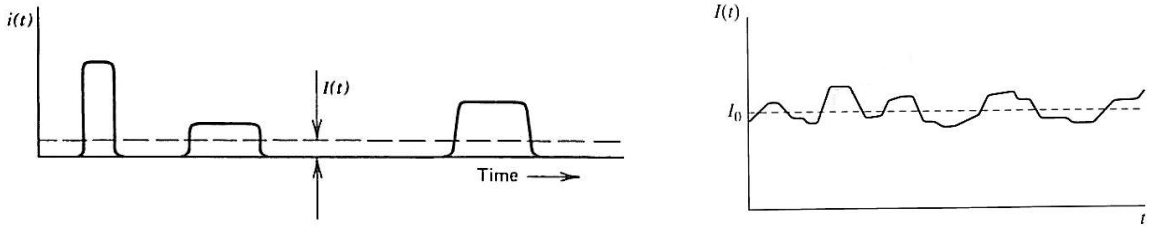

(a) (b)

FIGURE 2.5: **The current generated by a detector: 2.5(a) An example of the impulses read in this mode - the measured current is an average of the impulses within a time window and 2.5(b) the real value of the obtained current, without the small fluctuations, adapted from [2] .**

2.2.2 Pulse Mode

The pulse mode allow to obtain information about the amplitude and time of each produce event, and therefore we can estimate the produced charge. I allows to store the information of each quantum of radiation that interacts in the detector. In this method the detection is limited by signal-to-noise ration and by the radiation flux arriving to the detector, being

an advantage over other methods which the limits are imposed by the measurement of an average of interactions, i.e., current mode.

To perform the measurements, in this mode, the detector is typically connected to a charge sensitive preamplifier. The aim of such device is to convert the current signal produced inside the detector into a voltage signal. The total system (detector + preamplifier) can be summarized by the equivalent circuit shown in figure 2.6.

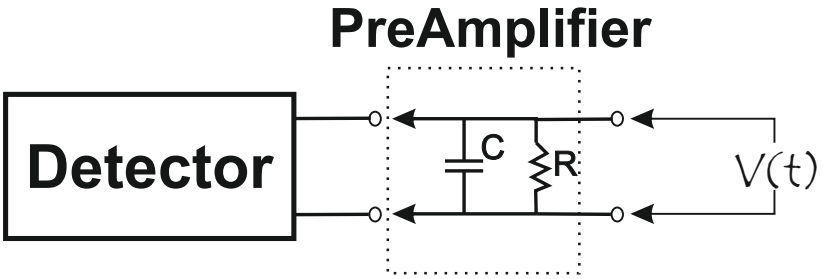

FIGURE 2.6: **An illustrative example of the equivalent circuit to operate in Pulse Mode. Here R the resistance of the Preamplifier and C the equivalent capacitance of the system (Detector + Preamplifier), adapted from [2].**

This configuration forces the system to do the conversion in a time τ, given by $\tau = RC$. There is other time constant related with the charge collection time (t_c). Evaluating both time constants and relating between them, is possible to identify two different cases.

In the first case, when $\tau \ll t_c$ the capacitor not have time to charge, therefore the current that flow across the resistor is equal to the current that leave the detector. This case is applied when the energy information is less important than the timing information/operation - figure 2.7(a). The measured voltage is given by the equation (2.1):

$$V(t) = Ri(t) \tag{2.1}$$

The another case, which is the used in this device, the current that leave the detector is integrated on the capacitor (capacitor charging) making the current that flow through the resistor, smaller. Then the capacitor will discharge, making the voltage drop back to zero. In each detected event, the voltage of the system increases during the time of the charge collection in the detector, not having any influence of external or load circuit. On other hand, the decreasing time only depends of the time constant of the system, the time τ.

The value of $V(t)$ is proportional to the collected charge and to inverse of the capacitance , being expressed in equation 2.2:

$$V(t) = \frac{Q}{C} \tag{2.2}$$

where C is the equivalent capacitance and Q the total charge collected (created within the detector).

2.3 The Measurements

2.3.1 Gain

After the successive charges multiplications in the detector, each photoelectron that leaves the photocathode origins an high number of electrons, ranging 10^5-10^6. The ratio between the total number of collected electrons and the number of electrons that leaves the photocathode

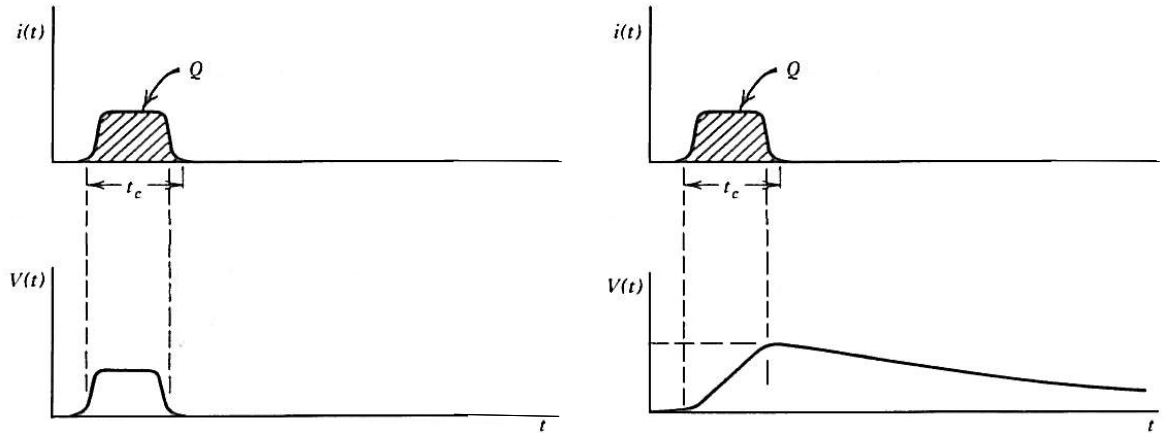

FIGURE 2.7: **An hypothetical example of the measured signal voltage $V(t)$ for: 2.7(a) the time constant of the circuit (τ) smaller than the time of the current pulse and 2.7(b) the time constant of the circuit (τ) larger than the time of the charge pulse. Adapted from [2] .**

is defined as *Gain*, being in this case exponentially proportional to the applied voltage, reflecting the exponential behaviour of the avalanche multiplication processes [2].

In this work the Gain was calculated by measuring the electron current that leaves the photocathode, also known as initial photocurrent - I_{PC0} and the current that is collected in anodes - I_{ANO}, and given by their ratio, as expressed by the following equation (2.3):

$$G = \frac{I_{ANO}}{I_{PC0}} \tag{2.3}$$

Figure 2.10 presents the schematic drawing of the measurements procedure. I_{PC0} was measured by applying an voltage difference between the Grid and the top of the THGEM1, producing an electron field for photoelectron extraction. To determinate the current, the voltage drop across a resistor of 10 MΩ was measured with a Fluke 233 multimeter. In this case, the TOP1 and BOT1 were at the same potential (0V), in order to ensure that the photoelectrons will be focused to the GRID and not to the THGEM1 holes.

For the measurement of I_{ANO} all the structures were polarized being the total collected charge acquired and measured through the voltage drop across a resistor of 10 MΩ with a Fluke 187 multimeter connected to the anodes. During this measurement the voltage in the THGEMs and the transfer fields were kept constant (V_{THGEM1} =530V, V_{THGEM2} =600V, $E_{TRANSF1}$ =0.33 kV/cm and $E_{TRANSF2}$ =0.27 kV/cm). In this case, the Grid was also connected to TOP1 in order to ensure a null drift field (E_{DRIFT} =0 kV/cm) in region between both. The gain curves were obtained varying V_{AC} and V_{CT}.

The entire system was prepared and set in order to avoid all movements that can compromise the measurements (for example, the lamp to detector position). The voltages were increased until the current value was higher than 50 nA. When this value was reached, an attenuator was placed over the quartz window, measuring again the current, in order to estimate the attenuation factor. This current limitation was used to prevent distortions in the electric field and to avoid discharges that, besides the robustness of the detector, can trigger secondary effects and affect the measurements.

2.3.1.1 Electronic Chain Calibration

The gain measurements can also be done in pulse mode, however the electronic chain must be calibrated, in order to measure, only, the detector contribution on the obtained spectra. Thus, the electronics chain calibration was performed by using the setup present in figure 2.8.

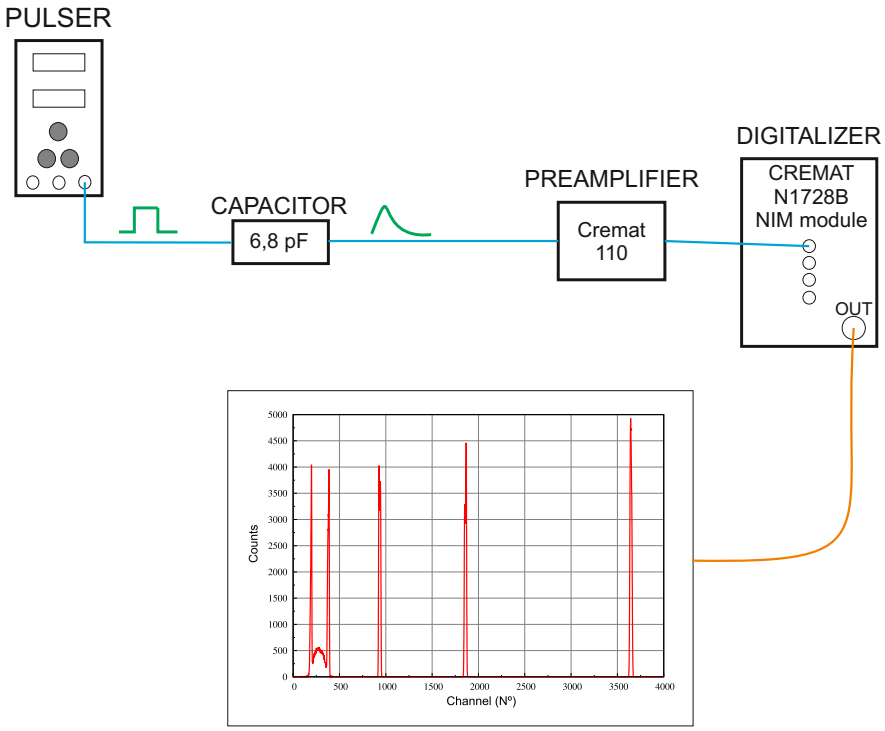

FIGURE 2.8: **Schematics of the electronic chain. For each voltage imposed by the Pulser, a charge pulse is collected in the Preamplifier, being digitized. .**

As illustrated in figure 2.8, we used a pulser to send a signal through the capacitor, simulating a typical detector pulse. This generated signal is then readthrough a CREMAT CR 110 (preamplifier), where it is converted in a voltage pulse and then sent to the CAEN N1728B NIM module digitalizer, which is connected to a computer allowing store the information.

The charge on the input of the preamplifier can be calculated by using the expression (2.4). By changing the amplitude of the generated pulse (in the Pulser), the charge on the input of preamplifier vary and therefore also the amplitude of the resulting pulse. At this point it is possible to relate the charge on the preamplifier input with the channel on the channel digitalizer (when operating as multichannel analyser), due to the obtained amplitude spectrum.

$$C = \frac{Q}{V} \tag{2.4}$$

Electronic chain calibration obtained results are shown in figure 2.9. In the real detector the charge collected in anodes is divided on the resistive line of the 2D-THCOBRA, and therefore the real calibration of the channels are the sum of the charge calculated through the calibration parameters of the two preamplifiers. Thus the equation (2.5) shows the relationship between the gain and the channel number.

$$Gain(channel) = 2345 \times channel - 62390 \tag{2.5}$$

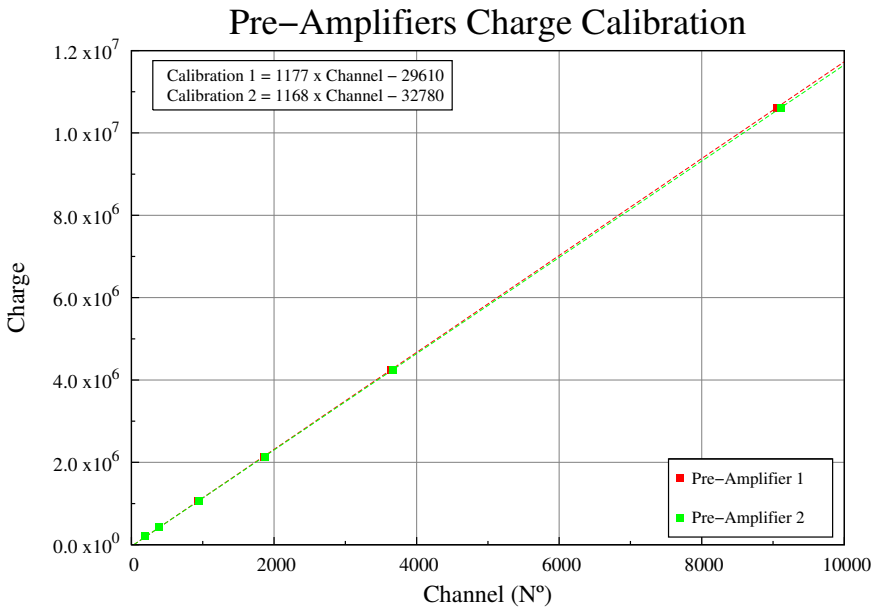

FIGURE 2.9: **Calibration curves of the preamplifiers used for gain calculations and image acquisition.**

2.3.2 Ion Back Flow - IBF

The process of charge multiplication is associated with successive ionizations in gas and as in any other ionization, when a electron is released a positive ion is formed. In each multiplication stage positive ions are created due to the gas ionization, being collected in different regions of the detector. The trajectory and the different places where occurs the collection are illustrated in figure 2.10(b). Due to the successive electric fields applied in the detector, the ions will move in opposite direction to the electrons, thus tending to reach the photocathode. This phenomenon led to a bombardment of the CsI layer by positive ions, cause the ageing of the photocathode, and therefore the decrease of quantum efficiency. Moreover, the ions movement may change the electric field locally, causing instabilities which can affect both, the image quality and the energy measurements or even trigger discharges inside the detector [16].

The Ion Back Flow (IBF) is defined as the fraction of produced ions in the charge multiplication processes that reaches the photocathode to the total charge collected in the anodes. IBF measurements were performed in current and calculated by the following expression (2.6):

$$IBF = \frac{I_{TOP1} - I_{PC0}}{I_{ANO}} \tag{2.6}$$

where I_{TOP1} is the current of the ions collected in photocathode, I_{PC0} represents the photoelectrons current and I_{ANO} is the current of electrons collected in the ANO. The I_{PC0} and I_{TOP1} currents are originated by opposite charges, however as their movements are also opposite, they are added. Thus is necessary to subtract the photoelectron current.

Similar to what described in section 2.3.1, the IBF measurements requires two steps. The first one is the measurement of I_{PC0} and the other one corresponds to the measurement of the I_{ANO} and I_{TOP1} measurements. The measurement of the I_{TOP1} and I_{ANO} currents were performed simultaneously. Also, in this case the measurements were performed by measuring the voltage drop across a 10 MΩ resistor with a Fluke 233 multimeter.

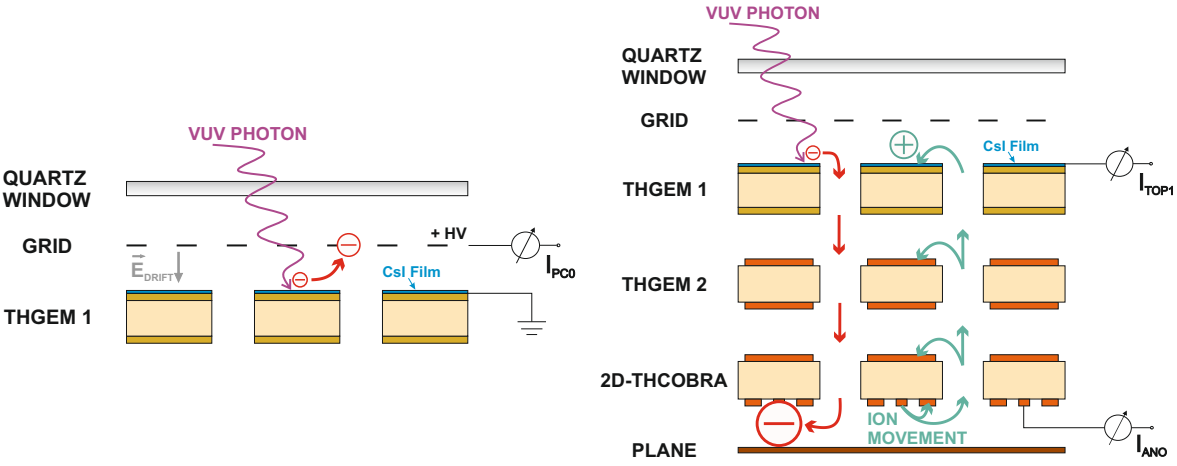

(a) (b)

FIGURE 2.10: **Schematic drawing of setup required to measure:2.10(a) I_{PC0} and 2.10(b) I_{TOP1} and I_{ANO}**

2.3.3 The Image Acquisition

The image acquisition is achieved by using a 2D-THCOBRA. The schematic drawing - Figure 2.11 - shows the setup used for the image acquisition. When an avalanche is collected, four signals are collected in both ends of each resistive lines, being converted in voltage signals by a CREMAT 110 preamplifier and digitalized by a CAEN N1728B NIM module, a four channels digitizer, with 14 bits and 100 MHz. The digitizer is connected to a computer which stores, processes and shows the results. The interaction position is determined by the method of the Principle of Resistive Charge Division - see section 2.3.3.1.

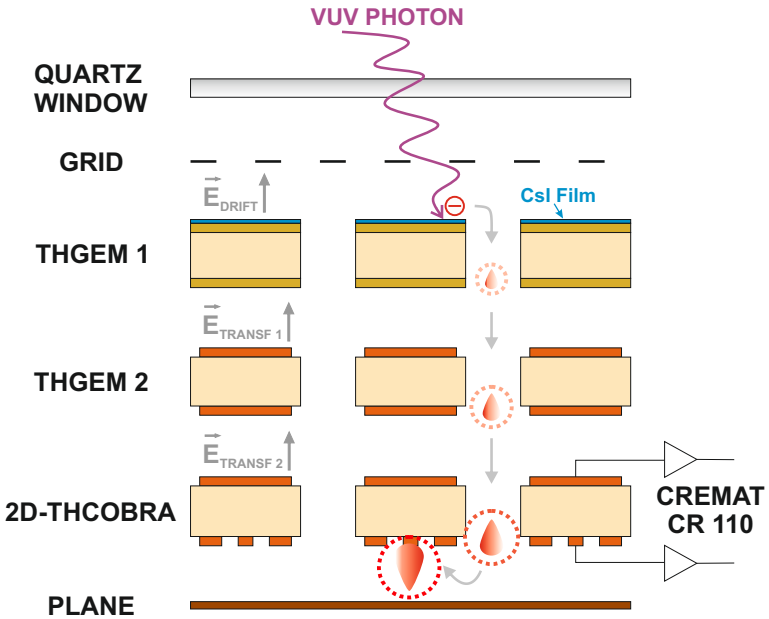

FIGURE 2.11: **Schematic drawing of the developed setup to obtain the signals in pulse mode.**

2.3.3.1 Principle of Resistive Charge Division

As mentioned, the charge produced by each event, is collected on the anode strips, that are connected through a resistive line. When the charge reach the resistive line it will be divided according to the principle of resistive charge division [31], being the interaction position determined, for one direction by the expression (2.7):

$$x = k\frac{X_L - X_R}{X_L + X_R} \tag{2.7}$$

where X_L and X_R are the amplitude of the signals collected in the edges (Right and Left side) of the resistive line of an electrode (TOPC or ANO), k is a calibration constant, associated with the length of the resistive line and x represents the calculated centroid position.

The orthogonal position is determined using the same principle. Denote that, in this case, the signal on the top strips is induced by the charge collection on the anode strips. This results on a smaller signal (about 60%) [31] with opposite polarity to the anodes signals.

The figure 2.12 resumes the acquisition and signals digitizing process.

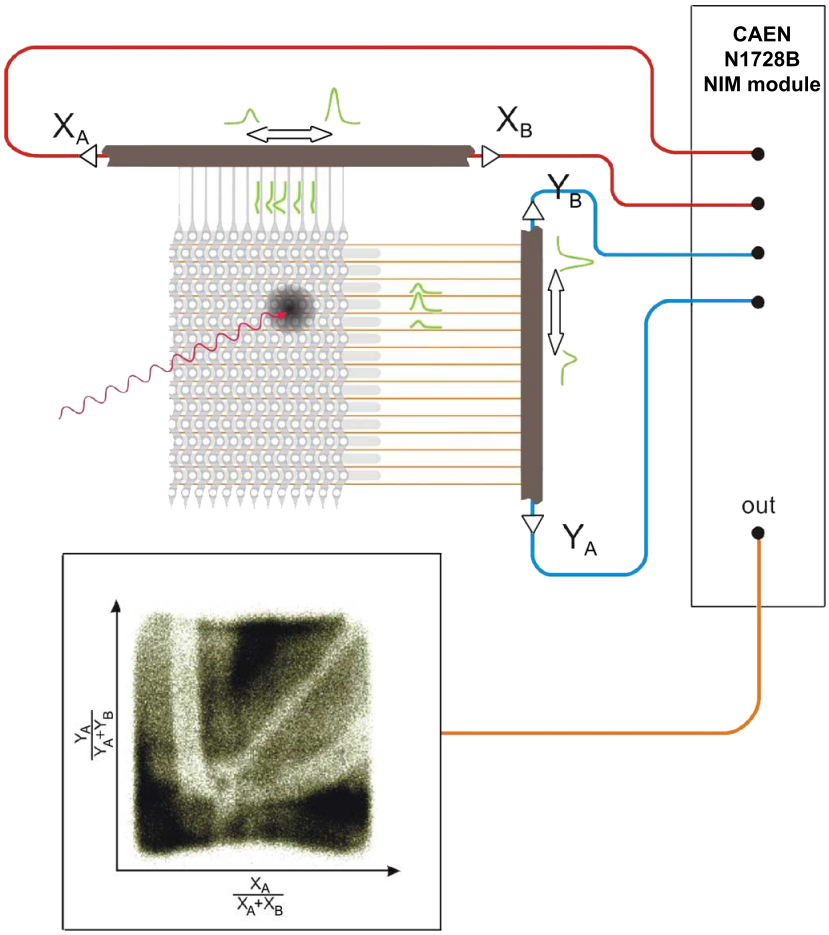

FIGURE 2.12: **Schematic drawing of the resistive charge division method. Each edge of the resistive lines contribute with a signal. Through signal amplitude can calculate the position of the collected avalanche, adapted from [31].**

2.4 Thermal Evaporation

Due to the values of photocathode QE presented in figure 1.2, the geometry chosen for this detector was the reflective geometry.

The deposition was done by using the vacuum evaporation chamber, existing in the department.

The first THGEM was placed in the center of the evaporation chamber cover, aligned with the filament boat. The THGEM was properly covered with a kapton mask in order to deposit the CsI photocathode only in the TOP electrode.

Then the chamber was closed starting the vacuum process, until the pressures reaches levels of about 10^{-6} mbar.

The deposition process starts with the pre-heat of the tungsten boat, by Joule effect, passing a 30 A current on the filament. Then the current was steeply increased until 100 A, approximately. At this point the CsI evaporation starts. The deposition velocity was controlled by a rheostat in order to not have rates higher than 40 Å/s. When the photocathode thickness is, approximately, 500nm the deposition process was stopped.

After a brief waiting time for the chamber cool down, the chamber is filled with air, being the substrate quickly transferred to the clean room, where the THGEM is mounted on the detector. This process should be as fast as possible in order to avoid the photocathode QE degradation by its exposure to air [32].

CHAPTER 3

Results

As we will see, this GPM and the entire experimental setup works like a normal single photon counting but also allows to obtain images, storing information related with the discrimination of the position as well as with the detector amplitude. Thus, through a simple acquisition we could have access to different information.

In the next sections, the results obtained for several characteristics of the detector, as Gain and IBF, will be present. Beside these, will also be present the imaging capability of this detector when operating with a resistive line readout implemented in the 2D-THCOBRA.

3.1 I_{PC0}

I_{PC0} is the current produced by the extracted photoelectron from the photocathode. This current was measured as a function of the electric field between the Grid and the TOP1, as illustrated in figure 2.10(a). In order to perform this measurement the TOP1 and the BOT1 were interconnect and both connected to ground. The high voltage was connected to the Grid, where the I_{PC0} current was measured. The results obtained are shown in figure 3.1.

For low values of electric field (∼below 200 V), not all of the extracted electrons can reach the mesh as the electrons do not have enough energy to escape from the photocathode or to overcome the backscattering effect (a photoelectron that collides with a gas atom and returns to the photocathode).

Between 200 and 600 V, the curves behaviour becames approximately linear with the electric field intensity. It was expected to observe a plateau in this region, although the observable small increase of the current is due to the extraction of deeper electrons from the photocathode result in the increase of the current.

Above the 600 V, the electrons have enough energy to excite the gas atoms and to promote the electroluminescence of the gas leading to a positive feedback due to the generation of new photoelectrons produced by the new generated photons.

The aim of the I_{PC0} is to determine the maximum photoelectron current extracted from the photocathode. Although the null electric field on the drift region, at the photocathode the surface electric field created by ΔV_{Hole} can be sufficiently high to maximize the photoelectron extraction. In such case we need to make an approximation considering the maximum photoelectron current as the average value of I_{PC0} plateau which is about 125 pA.

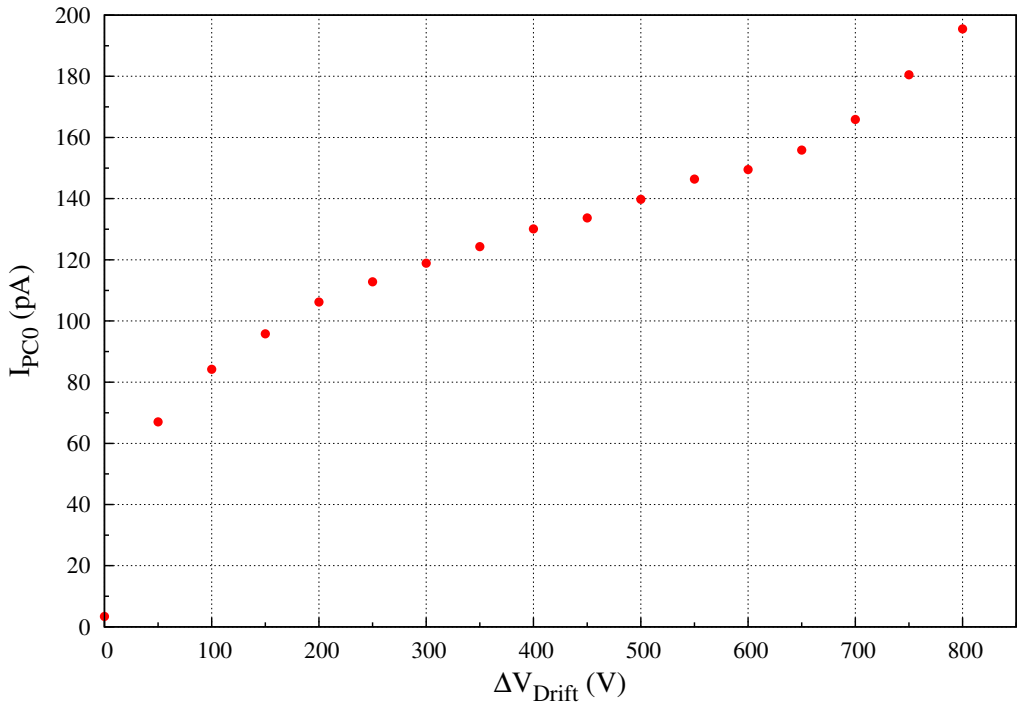

FIGURE 3.1: **I_{PC0} curve as a function of ΔV_{DRIFT}**

3.2 Gain

As mentioned in section 2.3.1, the Gain is calculated through the equation (2.3). The gain measurements were performed to evaluate the 2D-THCOBRA first and second charge multiplication. The results are illustrated in figure 3.2, showing the charge gain as a function of V_{AC} for several values of V_{CT}.

The results shown an exponential increase of the gain with the increasing of the V_{AC}, demonstrating the occurrence of the second charge multiplication on the anodes vicinity. Also demonstrating that this multiplication happens within the linear region of the graph 1.3.

It is also observed that the increasing of the V_{CT} results on higher gain values, which is expected due to the increase of the multiplication in the holes, similar to the THGEM behavior.

3.2.1 Gain Calculated in Pulse Mode

For the same conditions of the maximum gain obtained in current mode, i.e., V_{THGEM1} = 530 V, V_{THGEM2} =600 V, V_{CT} =570 V and V_{AC} =280 V, the transfer fields are also kept constant ($E_{TRANSF1}$ =0.33 kV/cm and $E_{TRANSF2}$ =0.27 kV/cm) and irradiated by the Hg(Ar) lamp, we measured the detector gain in pulse mode.

Since the detector was been operated in single-photoelectron mode, a typical single-photoelectron charge gain spectrum was obtained, being depicted in figure 3.3. This calculations were only be possible due to the electronic chain calibration done before this measurements and presented in section 2.3.1.1.

The figure 3.3 shows the typical Single-Photoelectron spectrum, following a Polya distribution, mathematically represented by the equation (3.1) [13]:

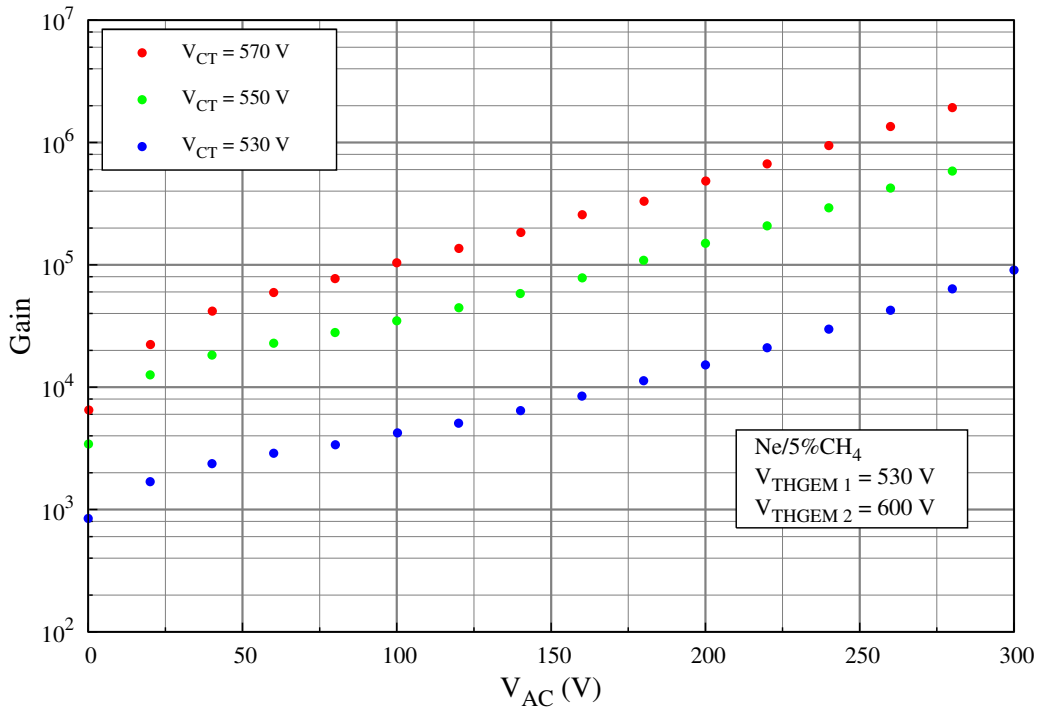

FIGURE 3.2: **Charge gain curves as function of V_{AC}, for different applied V_{CT} into the 2D-THCOBRA**

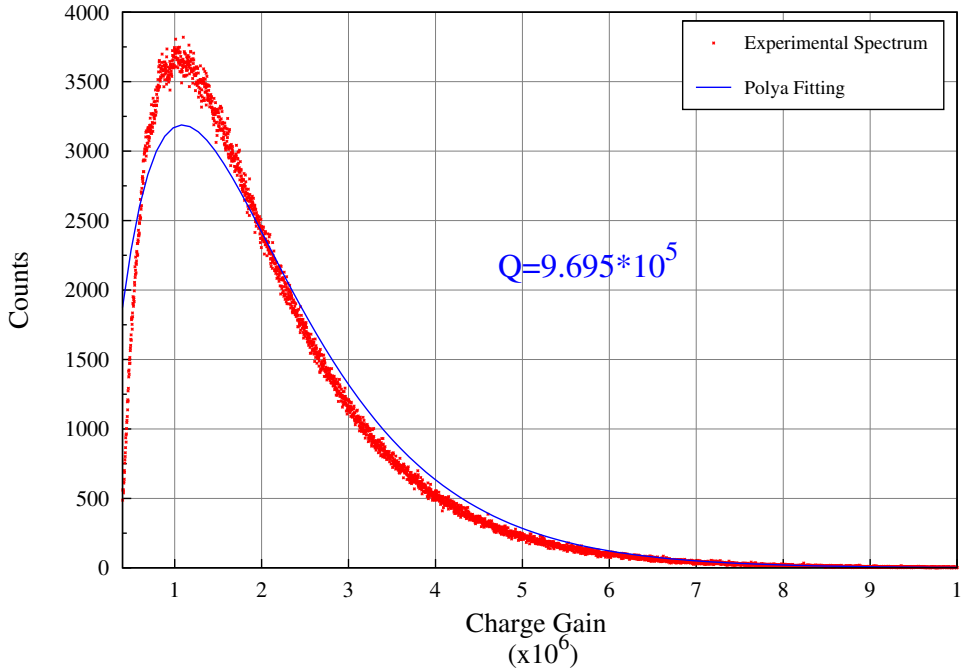

FIGURE 3.3: **A Single-Photoelectron energy spectrum, fitting to a Polya Distribution.**

$$P(q) = \frac{1}{Q} e^{-\frac{q}{Q}} \tag{3.1}$$

Through the fitting to a Polya distribution is possible to calculate the average detector charge gain. The value of the Q, illustrated in figure 3.3, is the detector gain calculated in pulse mode by the fitting to a Polya expression.

The calculated detector gain calculated, $Q = 9,695 \times 10^5$, using this methode is less than an half of the maximum gain obtained in current mode, and so, it can be conclude that the detector gain is about 10^6. This alternative method allows to achieve the same conclusions, being a complementary way to confirm the obtained results in current mode.

3.3 Ion Back Flow (IBF)

The reduction of IBF is important to avoid the photocathode aging, thus the study of IBF as function of V_{AC} for different values of V_{CT} was mandatory. Figure 3.4 presents the obtained results, using the setup and method described in section 2.3.2.

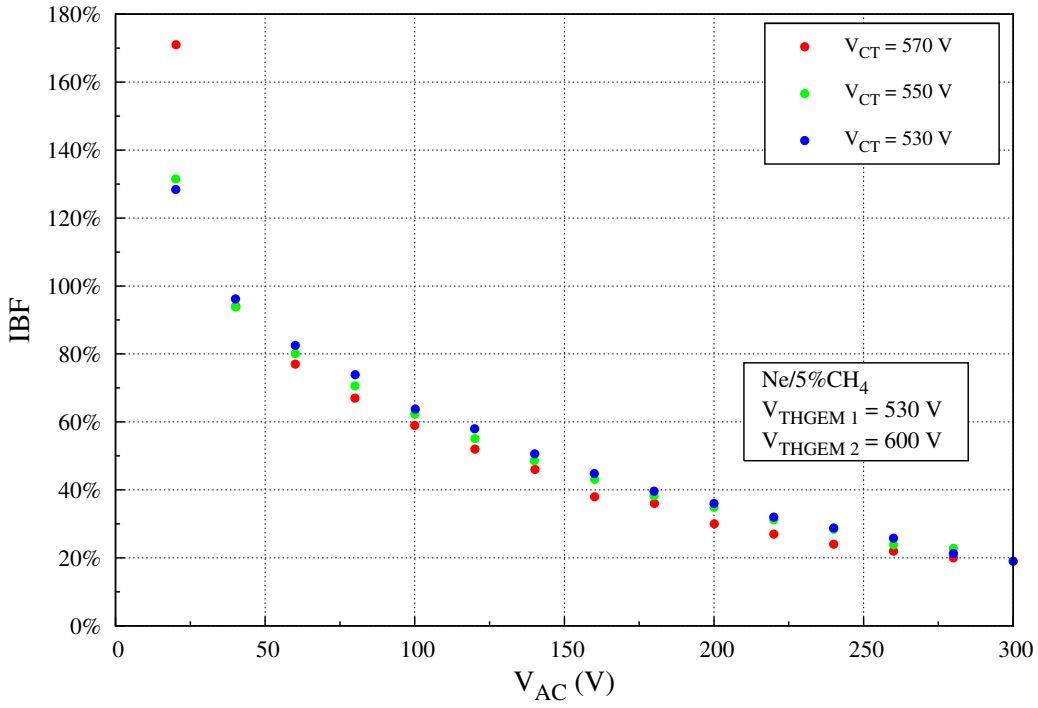

FIGURE 3.4: **Ion Back Flow curves as a function of V AC, for different VCT values, applied in the 2D- THCOBRA.**

A reduction of IBF with the increase of V_{AC} is observed due to the ion trap by the cathode strips. The figure also shows a tiny variation of the IBF with V_{CT} which means that, in principle, the IBF does not depend much on the gain in the holes.

For low values of V_{AC}, below 50 V the electric field is not high enough to promote an efficient drift to the anodes, resulting on a measured current (I_{ANO}) smaller than the effective current produced in the holes. This results on IBF values above 100%.

For V_{AC} values higher than 50 V the produced electrons that emerges from the holes start to be efficiently collected on the anode electrode where they are amplified. For V_{AC} values above 200 V, the IBF presents a variation between 40% and 20%.

Figure 3.5 presents the measured IBF values as a function of the total charge gain. As already mentioned, raising up the V_{AC}, will result on a 2D-THCOBRA gain increase. With

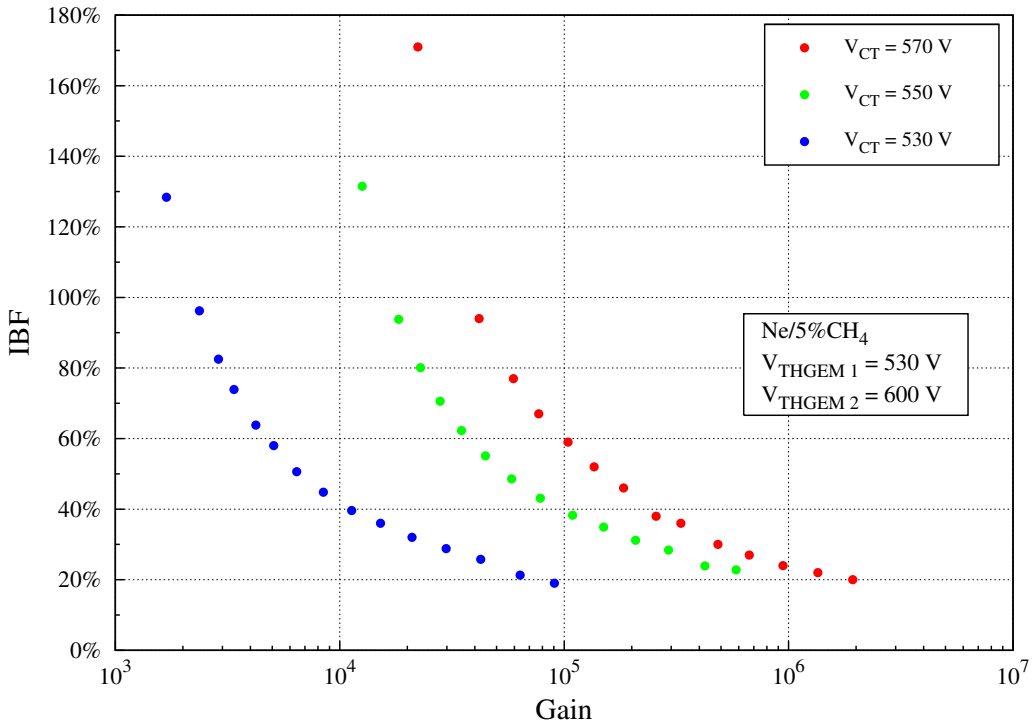

FIGURE 3.5: **Ion Back Flow as a function of the total charge Gain.**

the increase of the gain, the IBF tends decrease for each applied V_{CT} value. This means that, as expected, the ion trapping in cathode strips is effective. This allows increasing the final charge gain and at the same time keeping the number of ions that reach the photocathode at reasonable level. Although the number of ions that reach the photocathode increases, when the gain increases (more ions are formed during the avalanche processes) in the anodes vicinity, the effect of the ion trapping by the cathode also increases. In fact, when the avalanche take place near the anodes, the number of ions flowing back, that can be trapped on the cathode also increases.

In this study, the IBF have not reach IBF values comparable with the ones achieved with thin structures. To further improve the IBF some other techniques can adopted, as for example setting the induction plane voltage smaller than the cathode voltage, increasing the probability of collecting ions in the induction plane. Other option is to change the second structure to a reverse THCOBRA (R-THCOBRA) to further trap the ions that are flowing back from the last multiplication stages, as shown in ref [16].

3.4 2D-Imaging

The 2D-Imaging capability allows to determine the position where the final charge is collected, and this is only possible due to the organization of the TOPC and ANO electrodes into strips orthogonally disposed and using the principle of the resistive charge division, mentioned in section 2.3.3.1.

In order to obtain a 2D image, the entire sensitive area of the detector was irradiated by a Hg(Ar) lamp. For image acquisitions the applied voltages to the THGEM's were set to 530 V for the first THGEM and 600 V for the second one. The applied transfers fields were equal to $\vec{E}_{TRANSFER1} \simeq 0.33$ kV/cm and $\vec{E}_{TRANSFER2} \simeq 0.27$ kV/cm. The 2D-THCOBRA

was operated with V_{CT} =570 V and V_{AC} =280 V.

In the next subsections will be presented the image of the response and the spatial resolution of detector.

3.4.1 Single Photon Response

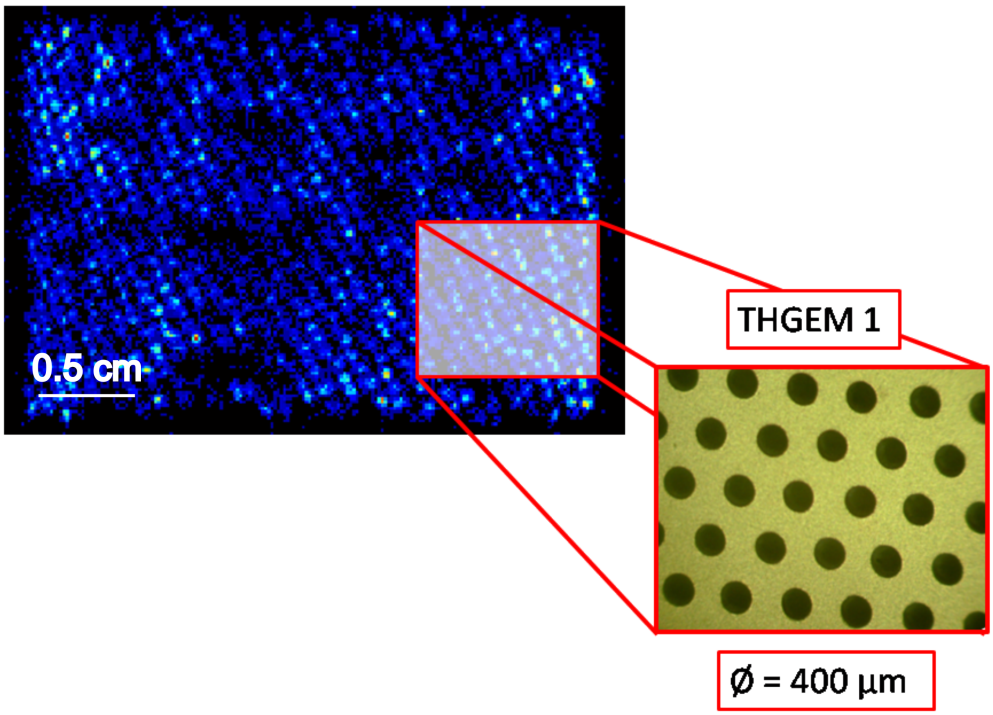

FIGURE 3.6: **a) VUV image of the detector sensitive area; b) Photo of the first THGEM, responsible for the pattern of the acquired images.**

Figure 3.6 shows one of the acquired images and a detailed view of the first THGEM.

As can be seen, the obtained image presents a hole pattern which results from the pattern of the first THGEM. The holes, in this structure, are hexagonally distributed with a pitch of 800 μm, as already mentioned. This hexagonal pattern is slightly rotated relative to the 2D-THCOBRA. However, the "shadow" of the first structure is not a feature exclusive of this image, being present in all of the acquired images.

The mentioned pattern can be eliminated from the images using different concepts or configurations. A structure with a lower pitch instead of the THGEM structure, as for example, a GEM can be used to reduce the effect. Another option would be to use a reversed-MHSP (R-MHSP), as first structure, since it would not only eliminate the pattern but also allows to further decrease the IBF [24].

In the obtained image it is possible to identify some variations in the intensity distribution across the sensitive area. These non-uniformities can be the result of local variations on the QE of the photocathode, related with some defects introduced during the deposition process. Other possibility is associated to local gain variations along the 2D-THCOBRA, generally related to the PCB substrate thickness variations and/or intrinsic non-uniformities introduced during the production processes, because the electric field is given by (3.2):

$$E = \frac{V}{d} \tag{3.2}$$

where E is the electric field, V the drop voltage applied between the electrodes and d the distance between them. Thus, for the same drop voltage across the structure, if the distance d varies, the electric field also change, occurring variations in the gain across the structure.

To evaluate the overall imaging response of the developed photosensor, another image, depited in figure 3.7, was obtained. However, in this case an UV mask was imaged, in order to test the performance of the detector for UV imaging. The UV mask contains several apertures with different sizes, being identified with numbers, figure 3.7. In order to obtain this image only a aperture number 3 were irradiated.

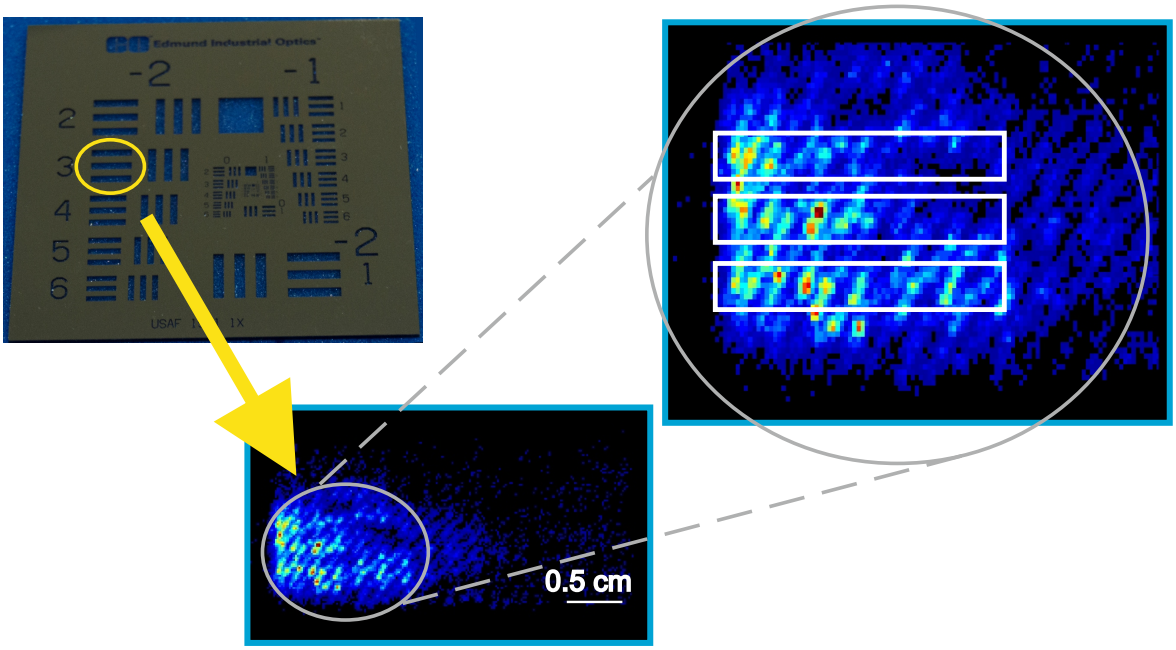

FIGURE 3.7: **The obtained VUV image from the mask**

Similarly to what happens in figure 3.6, figure 3.7 presents the THGEM1 hole pattern, becoming a limitation to identify, correctly, the UV mask. This is limited by the first structure pattern effect. Nevertheless, it is possible to identify the shape of the mask in the irradiated area.

These images, like the entire work, were obtained in single-photoelectron mode and they shown that 2D-THCOBRA is capable to produce good contrast images. This fact making it suitable for imaging applications, including low luminosity applications.

3.4.2 Local Gain

Using the possibility to store all information, gain spectrum as well as the interaction position, a study of the major influence of the non-uniformities shown in the obtained images, evaluating the local gain of the 2D-THCOBRA and the fluctuations of the gain on the detector, was performed. We divided the entire area of detection in a 20×20 matrix (each pixel corresponding to 1.4×1.4 mm^2), where each cell contains the information of the local energy spectrum. Then, a MATLAB script was created in order to fit each spectrum to a Polya distribution (equation 3.1) and return a value of the gain for each element of the matrix.

The image 3.8, shows the obtained matrix of spectrum and their fitting to a Polya distribution, like was done in figure 3.3 for the entire spectrum.

These fitting allow to map the detector gain and to evaluate the distribution of the gain in the 2D-THCOBRA. These results are presented in figure 3.9.

Figure 3.9(a) shows a two different regions with higher gain and between them a region of lower gain. The figure 3.9(b) shows that the more frequent charge gain is about $5,0 \times 10^5$ and a variation of $7,626 \times 10^4$, however this high value are related with the gain in the periphery.

Since we want to know if there is a relation between the intensity distribution in an image and the distribution of the gain along of the 2D-THCOBRA, we have obtained an image with 20×20 pixels, fully illuminating the detector uniformly with the UV lamp. The gain distribution and the intensity distribution are depicted in the figure 3.10.

By analyzing the figure 3.10 we can see that there is a relation between the gain distribution and the intensity distribution - the two higher gain regions corresponds to the higher intensity region, occurring the same for lower gain/intensity regions.

By comparing the figures 3.9(a) and 3.10(b) it is also possible to see similarities in the gain distributions, founding the same places for the higher gain regions, happening the same for the lower zones.

The observed relationship between intensity and gain distribution allow to understand the non-uniformities observed in figure 3.6, once the higher gain regions allow an higher signal-to-noise relation, and therefore a more image contrast, being possible to distinguish correctly the THGEM1 holes. Although it is the main reason for the non-uniformities, we cannot exclude the reason related with the QE of the photocathode, however this contribution should be very small due to the controlled uniformity during the evaporation process.

3.4.3 Spatial Resolution

Since we are limited to the hole pattern, resulted from the first THGEM configuration, we tried to use it in order to estimate a value for the spatial resolution offered by the 2D-THCOBRA structure. This pattern was analyzed for the parallel and orthogonal directions of the 2D-THCOBRA anode by selecting two orthogonal rectangular regions in the image and making their image projections, see figure 3.11.

The figure shows an example of a selected hole and the intensity projection distributions, corresponding to the cross sections selected, used to estimate the position resolution in both directions.

A Gaussian function was fitted to the intensity projection distributions and the Full Width at Half Maximum (FHWM) was determined for each distribution - see figure 3.12. The same procedure was applied for several selected regions for both directions. The average of the FHWM was 276 μm (σ =117 μm) for parallel direction (anode direction) and 300 μm (σ =128 μm) for the orthogonal direction (top electrode direction). The slight worse value obtained for position resolution using the top signals is because this signals are induced by the anode signal and therefore had a lower amplitude, being the signal-to-noise relation (SNR) also lower. Thus, there is slightly lower precision in the calculation of the avalanche position. Nevertheless, this difference is small and we can considered that both direction has about the same position resolution.

While the FWHM of these distributions does not represent the true spatial resolution of the system, the two parameters (FWHM and spatial resolution) are closely related and it is possible to infer that the spatial resolution is below the THGEM1 holes diameter, and certainly, below 300 μm.

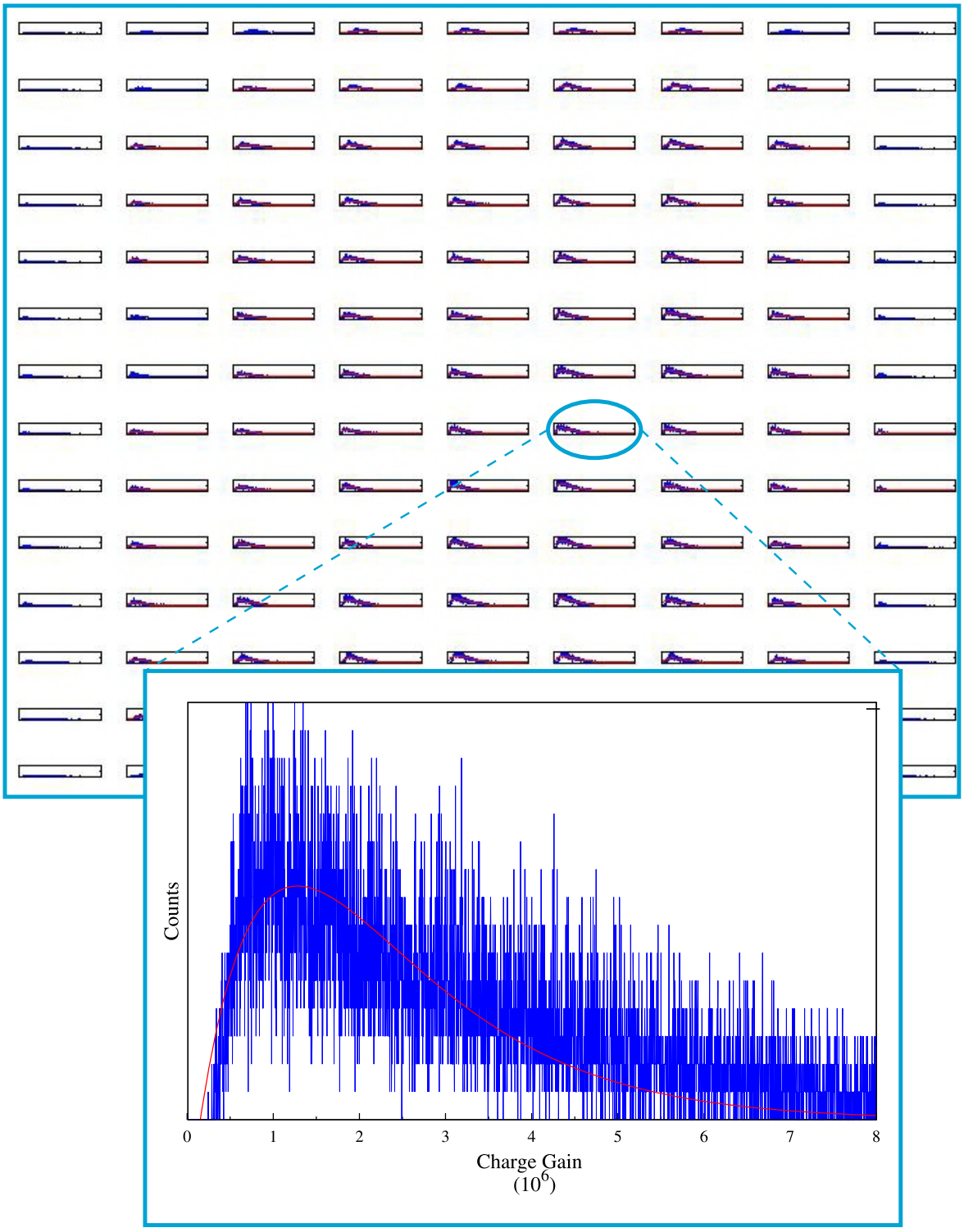

FIGURE 3.8: **20 × 20 Matrix of the gain spectrum of each detector zone with the fitting to a Polya Distribution, with a detailed view of a spectrum and the fitting.**

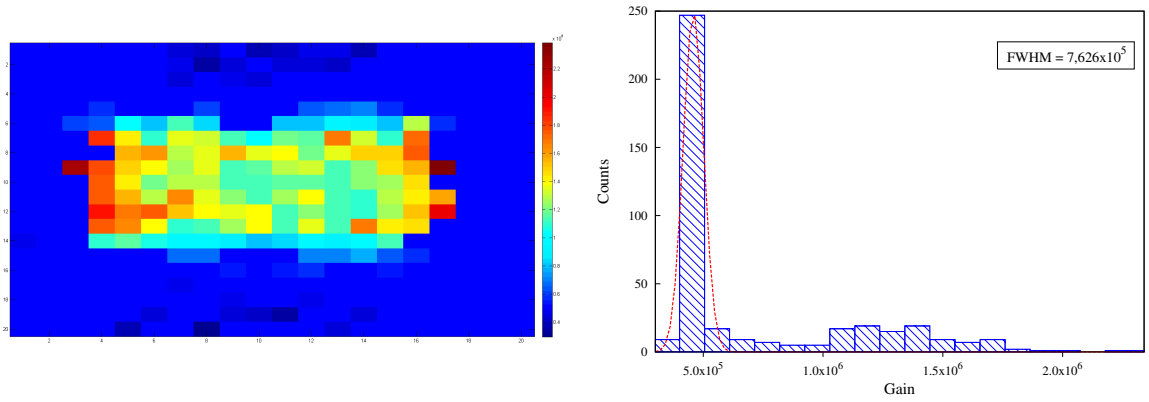

(a) (b)

FIGURE 3.9: **3.9(a) Gain distribution map of the 2D-THCOBRA for an example VUV image; 3.9(b)The histogram of the Gain variation presented in 3.9(a)**

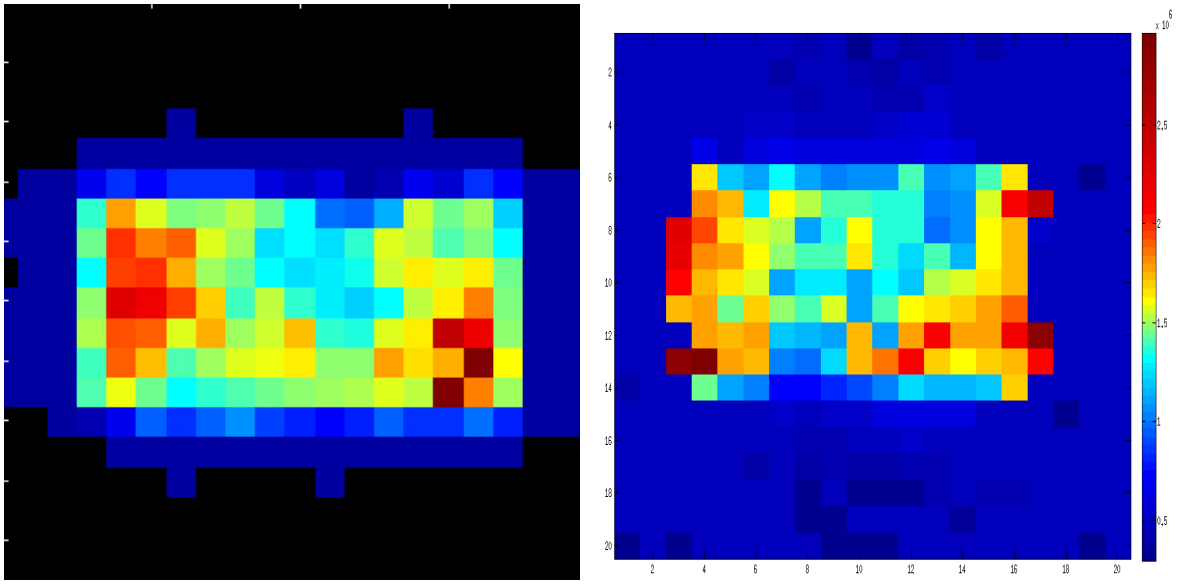

(a) (b)

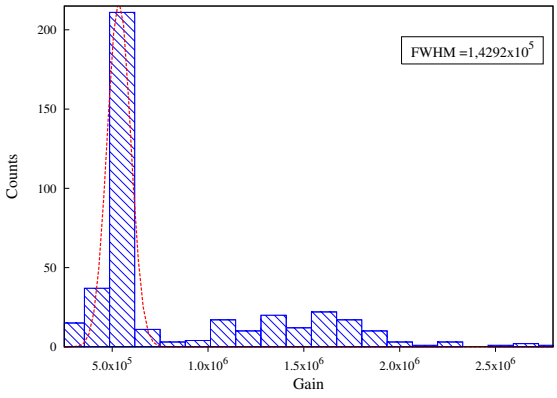

(c)

FIGURE 3.10: **3.10(a)An example of a 20 × 20 pixels VUV image of the detector sensitive area; 3.10(b) Gain distribution map of the 2D-THCOBRA, for the VUV image presented 3.10(a); 3.10(c) The histogram of the Gain variation presented in 3.10(b)**

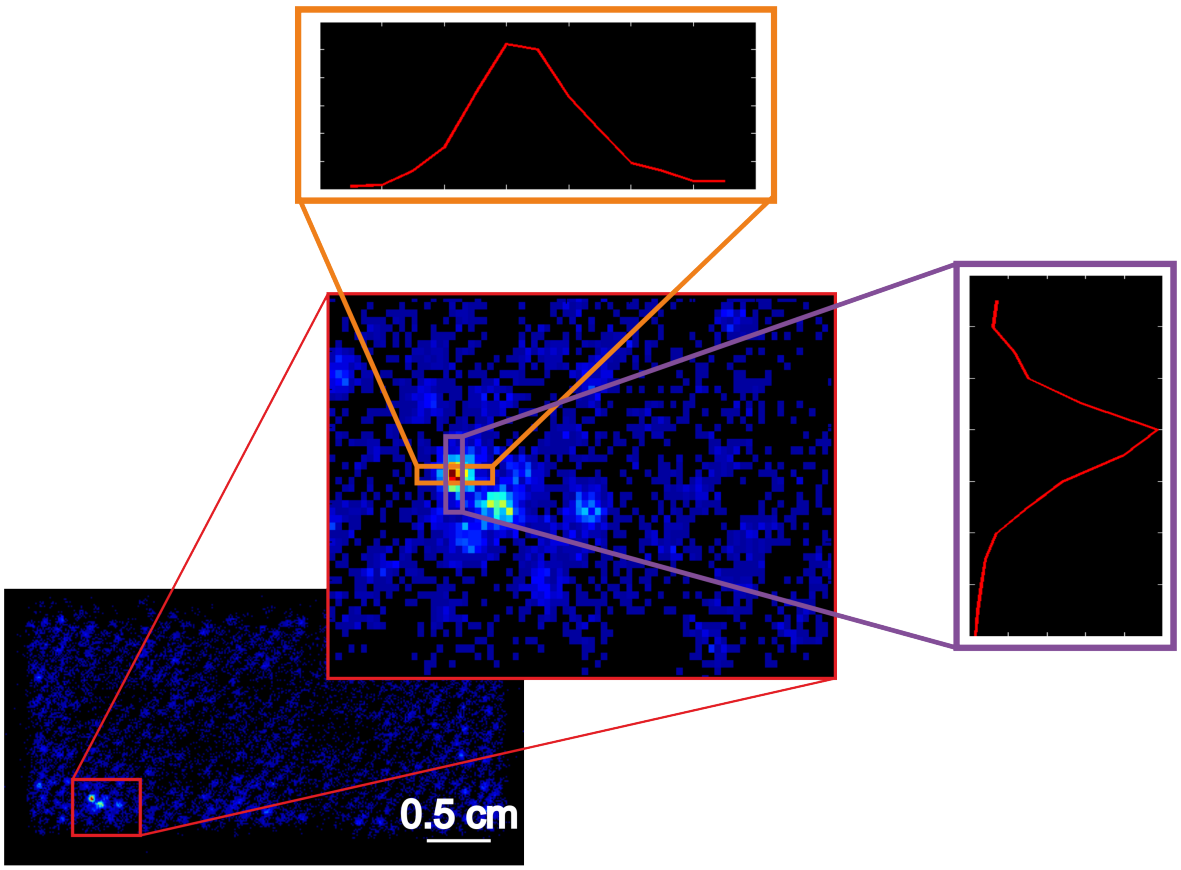

FIGURE 3.11: **a) Obtained VUV image of the detector entire active area; b) Detailed view of a small region selected in image; c1) and c2) Intensity distributions obtained for parallel and orthogonal to the anode direction,respectively.**

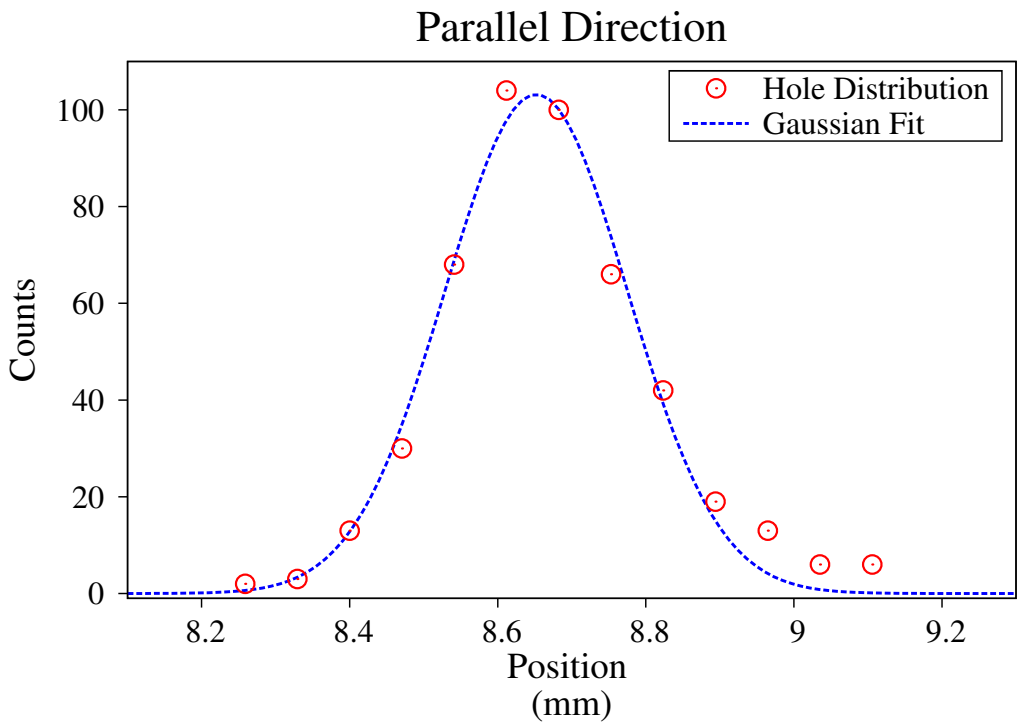

(a)

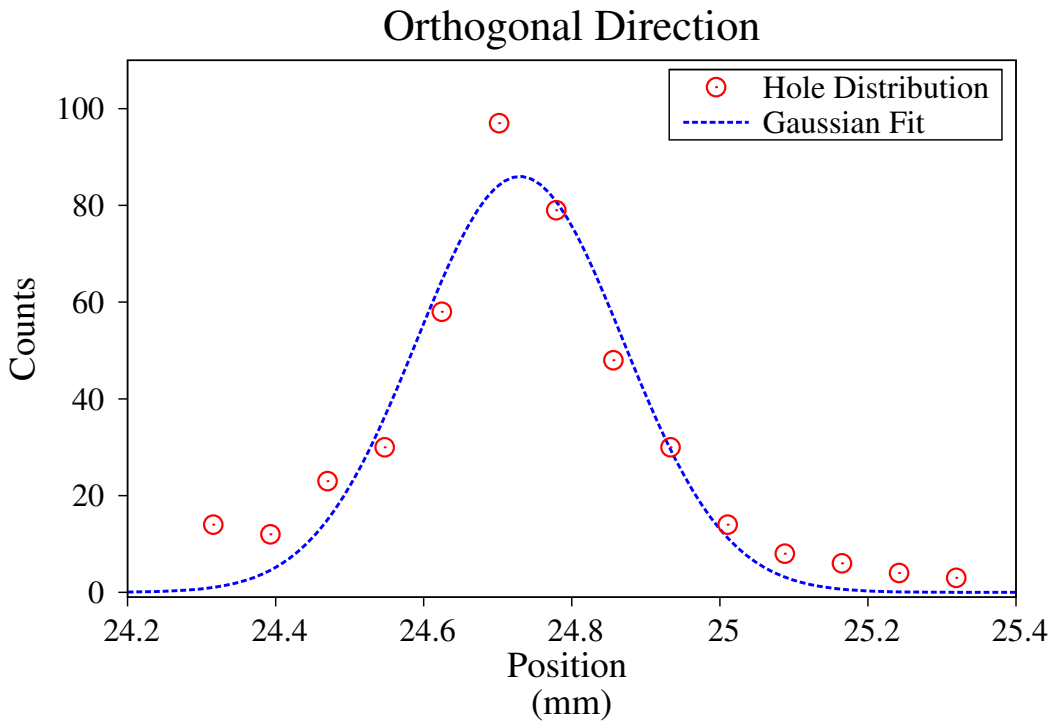

(b)

FIGURE 3.12: **Hole projection distribution and Gaussian fit for both directions: 3.12(a) Parallel direction – anode direction; 3.12(b) Orthogonal direction – top 2D -THCOBRA direction**

CHAPTER 4

Conclusion & Future Works

Along the present work a single photon counter, VUV sensitive, and presenting position detection capability, was developed, implemented and studied. It was demonstrated the good characteristics in terms of single photon detection and ion back flow reduction and position detection capabilities.

The Gain results shows the presence of a second stage of multiplication in the 2D-THCOBRA, which allows to increase the gain by a factor of 10-50 when compared with the standard THGEM, independently of the V_{CT} value. Thus, for the V_{CT} =570 V and increasing the V_{AC}, it is possible to obtain a gain 10^6 in single electron mode with a preamplification using two THGEMs. This results and the absence of discharges provide the detector stability and resistance requested for a GPM operation.

Besides the obtained high Gain value, the value of Ion Back Flow, responsable for an aging of the detector Quantum Efficiency was also studied and a first strategy for its reduction implemented. High values of IBF makes impossible the use of the GPM for detection in visible range, due to the secondary emission. With the proposed implementation, it was also shown that the second multiplication stage of the 2D-THCOBRA strongly influence the IBF value, since the increase of V_{AC} leads to IBF decrease, due to the higher collection on the cathode strips. With this configuration, values of IBF were reduced to about 20% of the total produced ions. This values can be further improved by, for example, using the THCOBRA in other levels in the cascade and with other configuration like as Reverse or Flipped-Reverse configuration.

The images obtained by the new Gaseous Photomultiplier shows a intrinsic pattern, resulting of the "shadow" of the first structure (THGEM 1). The pattern can be reduced using a higher granularity structure in the first position or depositing the photocathode film directly in the detector window.

The observed intensity distribution seen across the sensitive area found to be related with the local variation of the gain on the 2D-THCOBRA. In principle, the photocathode deposition uniformity, which can affects locally the photocathode QE, is not responsible for the variations on the observed intensity position distribution.

A quantitative analysis was performed for the intrinsic position resolution of the detector. FWHM values of 276 μm (σ =117 μm) for parallel direction (anode direction) and 300 μm (σ =128 μm) for the orthogonal direction, were obtained, leading to a high position resolution device when compared with other devices, e.g. Position Sensitive PhotoMultipliers Tubes,

which presents values in the millimeter scale [33, 34].

Taking into account all the results (Gain, IBF and spatial resolution) we can conclude that the new Gas Photomultiplier, based on 2D-THCOBRA, has great potential for imaging applications, such for high energy physics (e.g. RICH detectors), medical imaging and remote fire detection.

In future work, it will be considered to use higher granularity structures as the first structure in order to minimize the effect of the structure geometry or deposit the CsI photocathode in semi-transparent geometry.

Another goal will be further decrease of the IBF by using a R-THCOBRA or a F-R-THCOBRA as first/second structure in the cascade. In order to achieve both results can be used a reversed-MHSP (it has the same granularity of the GEM and allow the ion trapping in cathode electrodes). In this way, it may open the window for new types of GPM, using the better characteristics of both (thin and thicker) structures in the same detector, however it will be necessary to evaluate the immunity to discharges of this detectors and inquire the cost/benefice of this choice and the areas that can be covered.

Bibliography

[1] F. Flakus, "*Detecting and measuring ionizing radiation - a short story*", vol. 23, pp. 6, 1981.

[2] G. Knoll, "*Radiation detection and measurement*", Wiley, 2000.

[3] G. Charpak and F. Sauli, "*Multiwire proportional chambers and drift chambers*", Nuclear Instruments and Methods, vol. 162, no. 1–3, pp. 405 - 428, 1979.

[4] A. Oed, "*Position- sensitive detector with microstrip anode for election multiplication with gases*", vol. 263, no. 2-3, pp. 351-359, 1988.

[5] R. Bouclier et al., "*The Gas electron multiplier (GEM)*", vol. 44, no. 3, pp. 646-650, 1997.

[6] Y. Giomataris, "*Development and prospects of the new gaseous detector "Micromegas"*", vol. 419, no. 2-3, pp. 239-250, 1998.

[7] J. F. C. A. Veloso, J. M. F. Dos Santos and C. A. N. Conde, "*A proposed new microstructure for gas radiation detectors: The microhole and strip plate*", vol. 71, no. 6, pp. 2371-2376, 2000.

[8] S. Dalla Torre, "*Status and perspectives of gaseous photon detectors*", vol. 639, no. 1, pp. 111-116, 2011.

[9] K. Kurvinen, T. Collaboration and Ieee, Assembling of GEM detectors for the TOTEM experiment, pp. 597-602, Ieee, 2007.

[10] D. Neyret et al., "*New pixelized Micromegas detector with low discharge rate for the COMPASS experiment*", vol. 7, 2012.

[11] D. Di Bari et al., "*A large area CsI RICH detector in ALICE at LHC*", vol. 78, pp. 337-341, 1999.

[12] R. Chechik et al., "*Thick GEM-like hole multipliers: properties and possible applications*", vol. 535, no. 1-2, pp. 303-308, 2004.

[13] F. D. Amaro et al., "*The Thick-COBRA: a new gaseous electron multiplier for radiation detectors*", JINST, vol. 5, no. 10, pp. P10002, 2010.

[14] C. Azevedo et al., "*A Gaseous Compton Camera using a 2D-sensitive gaseous photomultiplier for Nuclear Medical Imaging*", Nucl. Instrum. Meth. A, vol. In Press, 2013.

[15] R. Chechik and A. Breskin, "*Advances in gaseous photomultipliers*", vol. 595, no. 1, pp. 116-127, 2008.

[16] J. F. C. A. Veloso et al., "*THCOBRA: Ion back flow reduction in patterned THGEM cascades*", Nucl. Instrum. Meth. A, vol. 639, no. 1, pp. 134-136, 2011.

[17] A. L. M. Silva et al., "*X-ray imaging detector based on a position sensitive THCOBRA with resistive line*", vol. 8, no. 05, pp. P05016, 2013.

[18] M. A. Nitti et al., "*Progress in the production of CsI and diamond thin film photocathodes*", vol. 553, no. 1-2, pp. 157-164, 2005.

[19] A. Breskin, "*CsI UV photocathodes: History and mystery*", vol. 371, no. 1-2, pp. 116-136, 1996.

[20] A. Breskin et al., "*Advances in gas avalanche photomultipliers*", vol. 442, no. 1–3, pp. 58-67, 2000.

[21] M. Hoch, "*Trends and new developments in gaseous detectors*", vol. 535, no. 1-2, pp. 1-15, 2004.

[22] H. Luz, "*Development of neutron and X-ray imaging detectors based on MHSP*", University of Aveiro, Aveiro, Portugal, 2009.

[23] J. M. Maia et al., "*Avalanche-ion back-flow reduction in gaseous electron multipliers based on GEM/MHSP*", vol. 523, no. 3, pp. 334-344, 2004.

[24] A. Breskin et al., "*Ion-induced effects in GEM and GEM/MHSP gaseous photomultipliers for the UV and the visible spectral range*", vol. 553, no. 1–2, pp. 46-52, 2005.

[25] H. Luz et al., "*MHSP with position detection capability*", vol. 573, no. 1-2, pp. 191-194, 2007.

[26] A. Breskin et al., "*A concise review on THGEM detectors*", vol. 598, no. 1, pp. 107-111, 2009.

[27] M. Alexeev et al., "*The quest for a third generation of gaseous photon detectors for Cherenkov imaging counters*", vol. 610, no. 1, pp. 174-177, 2009.

[28] T. Lopes and al., Position sensitive VUV gaseous photomultiplier based on Thick-multipliers with resistive line readout.

[29] Spectrosil Quartz Window.

[30] Spectral Calibration Lamps.

[31] H. Luz et al., "*Single Photon Counting X-Ray Imaging System Using a Micro Hole and Strip Plate*", vol. 55, no. 4, pp. 2341-2345, 2008.

[32] J. Almeida et al., "*Microanalysis surface studies and photoemission properties of CsI photocathodes*", vol. 367, no. 1-3, pp. 337–341, 1995.

[33] Z. W. Fu et al., "*A position-sensitive detector with lithium glass and MaPMT*", Chinese Physics C, vol. 36, no. 11, pp. 1095-1100, 2012.

[34] R. T. Souza, Z. Q. Gosser and S. Hudan, "*Using induced signals to sense position from a microchannel plate detector*", Review of Scientific Instruments, vol. 83, no. 5, 2012.